An Investigation of Atmospheric Temperature, Humidity and Cloud Detection Techniques Over the Arctic Marine Cryosphere.

Lauren M. Candlish

A thesis submitted to the Faculty of Graduate Studies of
the University of Manitoba
in partial fulfilment of the requirements of the degree of

Master of Science

Department of Environment and Geography
University of Manitoba
Winnipeg

Abstract

The veracity of a Radiometric Microwave Profiling Radiometer (MWRP) while mounted onboard a ship in the Arctic marine environment was assessed. The MWRP was validated against radiosonde data by calculating the root-mean-square difference and bias for simultaneous measurements taken for both temperature profiles and absolute humidity profiles. The vertical resolution of the MWRP was calculated using the inter-level covariance method. Based on the comparisons, the MWRP provided reliable measurements of both temperature and absolute humidity while mounted on the CCGS Amundsen.

Satellites CloudSat and Calipso's data products were assessed over the Arctic marine cryosphere. Temperature and absolute humidity from the ECMWF-aux data product was compared with profiles from the ship based microwave profiler. The cloud base heights measured by the ceilometer and MWRP were compared to CloudSat and Calipso's combined data product, GeoProf-lidar. Due to a large number of possible false detections, the constraints used by the GeoProf-lidar data product for cloud detection may need to be further refined.

Acknowledgements

I would like to thank my supervisor, Dr. David Barber, and my graduate committee members, Drs. John Hanesiak and Paul Bullock. Without their support and ideas this would not have been possible.

I would like to extend my thanks and appreciation to John Iacozza, Matt Asplin, and Rick Raddatz for their guidance and assistance. I would like to thank all my co-workers and friends for their considerable help through this process.

I would also like to acknowledge the following organizations for their support: the Circumpolar Flaw Lead System Study, the ArcticNet program of the Network of Centres of Excellence and the Northern ScienceTraining Program.

Dedications

To my father Christopher Candlish, without your support, your expert knowledge of graphic design and your countless hours editing this would not have been possible. To my mother Jacqueline Candlish, for all her love and support.

To Matt Gale, for his support and encouragement.

Contents

List of Figures

List of Tables

1 Introduction

The rapid changes we recently observed in the Arctic may give a glimpse of the changes that are likely to occur elsewhere in the coming years. Polar amplified winter temperatures in Alaska and Western Canada have risen as much as 3-4 degrees Celsius over the past 50 years (Turner et al., 2007). Although the Arctic climate varies greatly from year-to-year and from region-to-region, changes in air temperature and sea ice show that the pace of Arctic climate warming is greater in recent years than in the 20th century.

Clouds have a large effect on the solar radiation exchange at the surface, making them a critical part of the Arctic climate system. Kay and Gettelman (2009) conclude that changes in cloud cover due to sea ice loss will effect the ice-albedo feedbacks during summer, and may also contribute to the cloud-ice feedback during early fall. Curry et al. (1996) stress that to understand and simulate the cloud-radiation feedback mechanism there must first be an in depth understanding of the changes that occur in cloud properties, particularly, cloud fractional coverage and vertical distribution of the temperature and humidity.

The difficulty and expense of mounting field programs in the Arctic gives reason that satellite data for detection and measurement of cloud parameters is widely used. CloudSat's 94-Ghz cloud profiling radar (CPR) and Calipso's (Cloud-Aerosol Lidar and Infrared Pathfinder Satellite Observation) 532 nm and 1064 nm Cloud-Aerosol Lidar with Orthogonal Polarization (CALIOP) lidar are the first satellites with the capability to vertically profile the structure of Arctic clouds. The combined radar-lidar cloud detection technique relies on the backscattered energy from the cloud

particles. The weak thermal and albedo contrasts between clouds and the ice-covered Arctic surface make other cloud detection techniques insufficient in the Arctic due to their reliance on passive radiances.

The main objective of this study is to determine whether CloudSat and Calipso's data products can be reliably used to study cloud processes in a high latitude polar environment.

Validation and data inter-comparison is important to determine the quality of the satellite data in terms of how well it agrees with well established reference data for every circumstance and every season. Data inter-comparison is also needed to obtain clues as to how to solve protruding differences with reference data as feedback to algorithm developers and to monitor the degradation of satellite instruments. Validation is essential to users and developers and required during the whole lifetime of the satellite's instruments.

In order to validate satellite data products this thesis uses the method of statistical comparisons with standards. With this type of validation ground based systems, networks and balloons are used for comparisons of the satellite data. Statistical comparisons were done focusing on the differences. The statistics on the mean, median, RMS difference and bias were performed, with plots of the differences.

Field data were collected during two campaigns, the Circumpolar Flaw Lead System Study, 2008 and the ArcticNet Cruise 2009. Both campaigns were supported by the Canadian Coast Guard Ship (CCGS) Amundsen and were based in the Beaufort Sea and Amundsen Gulf. Due to the nature of comparing data from a satellite and a

mobile ship two continuously monitoring instruments were used, a Radiometrics Microwave Profiling Radiometer (MWRP) and a Vaisala CT25K ceilometer. Since the MWRP was first purchased in 2007 and used a neural network that was trained using historical radiosonde data based out of Inuvik, NWT, Canada, the acuracy of the MWRP data first needed to be assessed. Chapter two is a manuscript that examines the accuracy of a Radiometric Microwave Profiling Radiometer while mounted onboard a ship in the Arctic marine cryosphere.

The MWRP provides high temporal resolution atmospheric profiles for temperature, and absolute humidity up to 10 km. Sixty-eight radiosondes were launched over sea ice and the open ocean during the Circumpolar Flaw Lead System Study (CFL), 2008 and the ArcticNet Cruise, 2009, in the Western Canadian High Arctic. The data was categorized into seasons and further stratified by underlying sea ice concentrations. The MWRP was validated against the radiosonde data by calculating the root-mean-square difference and bias for simultaneous measurements taken for both temperature profiles and absolute humidity profiles. The temperature biases for each season were consistently positive, indicating that the MWRP recorded lower temperatures than the radiosondes. The calculations that account for varying degrees of sea ice cover indicate that there is a larger bias when there are low concentrations of sea ice present. The vertical resolution of the MWRP was calculated using the inter-level covariance method. The vertical resolutions calculated were in general as coarse as the height measured; at a height of 1 km the vertical resolution was approximately 1000 m.

To address the overarching objective of this thesis chapter three is a manuscript that looks at the use of CloudSat and Calipso, to vertically profile clouds in the Southern Beaufort Sea. The manuscript compares temperature and absolute humidity as measured by the MWRP with CloudSat's data product ECMWF-aux. It also looks

at the cloud base heights measured by the ceilometer and MWRP and compares them to CloudSat and Calipso's combined data product GeoProf-lidar.

CloudSat's ECMWF-aux product uses data produced by the European Center for Medium Range Weather Forecasting (ECMWF) and is interpreted into CloudSat's vertical bins. Temperature and absolute humidity from the ECMWF-aux was compared with profiles from the ship based microwave profiler. During each season the temperature bias was generally negative, indicating that the ECMWF-aux data was measuring warmer temperatures. The RMS differences for temperature were relatively large. This indicated that CloudSat's ECMWF-aux temperature profiles should be viewed with scepticism. The absolute humidity during spring and summer showed relatively large RMS differences from the surface to 2 km and should be viewed as suspect.

Statistical analysis was performed on CloudSat and Calipso's cloud base height data product (GeoProf-lidar) and compared with the microwave profiler and ceilometer data. Cloud height and cloud occurrence is tremendously variable over short distances. Data was compared when the satellite's ground track was within 50 km of the Amundsen's location. There were fifteen discrepancies when the ship based ceilometer and MWRP indicated clear skies for six hours and the GeoProf-lidar measured clouds. This is an indication that the constraints used by the GeoProf-lidar data product for cloud detection may need to be refined to reduce the large number of possible false detections.

Chapter four is a concluding chapter which summarizes the findings of the two manuscripts and presents future directions.

Appendix A is an in depth description for each of the instruments used.

Appendix B is an analysis of the ceilometer to verify that the data, prior to a routine calibration in March 2010, were valid.

Veracity of Atmospheric Temperature and Absolute Humidity Profiles over the Beaufort Sea and Amundsen Gulf from a Microwave Radiometer

Lauren M. Candlish

Richard L. Raddatz, Matthew G. Asplin and David G. Barber

Submitted to the Journal of Atmospheric and Oceanic Technology

December 10, 2010.

Manuscript No. JTECH-D-10-05050

2 Veracity of Atmospheric Temperature and Absolute Humidity Profiles over the Beaufort Sea and Amundsen Gulf from a Microwave Radiometer

This chapter is a paper submitted for publication to the Journal of Atmospheric and Oceanic Technology. This manuscript is a comparison of temperature and humidity measurements from a Radiometrics microwave profiling radiometer (MWRP) and radiosondes. The MWRP was mounted onboard a mobile ship in the Arctic which required validation with the radiosondes which have a long history and are considered the standard for atmospheric profiling. The co-author's are Rick Raddatz, Matt Asplin and David Barber. Rick Raddatz was involved in developing the statistical methods and the editing of the manuscript. Matt Asplin helped with the collection of the field data and post processing of the raw MWRP data, as well as editing the manuscript. David Barber provided funding for this research, contributed to ideas through his supervisory role, and contributed edits to the manuscript.

2.1 Introduction

In recent years, there has been an increased interest in accurately modeling Arctic weather and climate. Several large research projects have been undertaken to achieve a better understanding of the 3-dimensional structure of the Arctic atmosphere and its seasonal patterns. These projects included the Circumpolar Flaw Lead System Study (CFL) and the ArcticNet Cruise. The CFL project, from October 2007 to August 2008, was an over wintering field campaign in the Amundsen Gulf (70.5 °N; 124.0 °W) supported by the Canadian Coast Guard Ship (CCGS) Amundsen, Canada's research icebreaker (Barber et al., 2010). The 2009 ArcticNet Cruise occurred from July to November 2009 in the Beaufort Sea, and was also supported by the CCGS Amundsen. The Circumpolar Flaw Lead Study and the ArcticNet Cruise 2009 provided a unique opportunity for the validation of a Radiometrics profiling radiometer, which provided high frequency monitoring, during all seasons in the Western Canadian Arctic. Microwave radiometric profilers have been operated and tested at a variety of locations around the world, including Linkenholt UK, Lindenberg Germany, Payerne Switzerland, Oklahoma, Kansas, Washington and Alaska USA. Gaffard et al. (2008) found that in Likenholt UK the radiometer profiles decreased in accuracy with height. Using data from Lindenburg, Germany and Lamont, Washington, USA, Ware et al. (2003) observed that the microwave radiometer profiles are smoother than radiosonde profiles; this is a result of the microwave radiometer giving volumetric measurements while the radiosonde gives point measurements.

This paper examines the use of a Radiometrics TP/WVP 3000 microwave profiling radiometer (MWRP) in the Amundsen Gulf and Beaufort Sea. Field data were collected over sea ice and the open ocean during the Circumpolar Flaw Lead System

Study, 2008 and the ArcticNet Cruise, 2009, in the Western Canadian High Arctic. Throughout the CFL project, 65 weather balloons carrying Vaisala radiosondes (RAOBS) were launched while the Radiometrics microwave profiling radiometer produced continuous vertical profiles of the atmosphere from the surface to 10 km from November 2007 until July 2008. The second field campaign supported by ArcticNet onboard the CCGS Amundsen provided an additional 48 radiosonde profiles plus continuous MWRP profiles from July 2009 until November 2009.

The objective of this paper is to determine how reliable the MWRP is when mounted onboard a mobile ship in the high Arctic. The first part of this objective is to statistically compare coincident radiosonde measurements to the MWRP measurements taken for temperature and absolute humidity from the surface to 10 km in height. The second part of this objective is to investigate whether the performance of the MWRP, when profiling the boundary layer of the Arctic atmosphere, varies based on surface sea ice conditions.

2.2 MWRP Description

The Radiometrics TP/WVP 3000 microwave profiling radiometer provides high temporal resolution ($\approx$ 1 minute) atmospheric profiles for temperature (K), and absolute humidity (10^{-3} kg m^{-3}) up to 10 km. The MWRP onboard the CCGS Amundsen was mounted behind the bridge near the smoke stack, Fig. 1. The MWRP uses passive microwave radiometry for water vapor and temperature profiling. The instrument contains sensors to measure surface pressure, surface temperature, and surface relative humidity. The MWRP also contains a zenith-pointing infrared radiometer (9.6 – 11.5 μm), to provide the cloud-base altitude. The profiles are processed in real-time giving continuous monitoring of the lower troposphere, interrupted only by accumulation of liquid water on the radome during moderate to heavy precipitation.

Solheim et al. (1998), Guldner and Spankuch (2001), Ware et al. (2003), and Gaffard et al. (2008), provide complete descriptions of the radiometric profiling of temperature and water vapor, so only a brief description is provided. The MWRP views atmospheric radiances from the zenith direction in 12 channels. The five channels between 22-29 GHz provide information on the water vapor profiles, while the seven channels in the oxygen band (51-59 GHz) provide information on the atmospheric temperature profile. The water vapor profiling channels are calibrated hourly with tipping curves (Guldner and Spankuch, 2001). An external liquid nitrogen blackbody target is used to intermittently calibrate the temperature channels. All 12 channels perform a relative calibration every 5 minutes by viewing an internal black body target.

The MWRP provided temperature and humidity values that are volumetric measure-

Figure 1: The MWRP mounted onboard the CCGS Amundsen.

ments at 50 meter intervals for 0 to 0.5 km, 100 meter intervals for 0.5 to 2 km, and 250 meters for 2 to 10 km. The values are derived from microwave brightness temperatures using the Radiometric's neural network retrieval and radiative transfer model. The neural network is trained by historical radiosonde data from the upper-air station in Inuvik, N.W.T., Canada (68.30 °N; 133.47 °W). While the location of Inuvik is approximately 100 km from the coastline, it is the closest location that has a sufficient number (hundreds) of historical radiosondes to train the neural network. Due to the neural network being trained by land based radiosondes there was some concern that the MWRP profiles would have a bias when it was located on a ship in a marine environment.

The ship-borne MWRP may show a bias, however in the arctic marine environment the sea ice cover can act as a barrier limiting the exchange of latent and sensible heat, in addition to the exchange of water vapour between the ocean and atmosphere. The sea ice surface, when thick enough, creates a thermal barrier between the ocean and the atmosphere (Barry et al., 1993). During the cold months new ice with thickness of 0 – 0.4 m still allow heat fluxes of 1 and 2 orders of magnitude larger than that from perennial ice. Once the ice thickness exceeds 1.0 m the total heat flux through the ice remains constant (Maykut, 1978). Although the sea ice can reduce the amount of latent and sensible heat being transferred between the ocean and the atmosphere, this is very dependent on the time of year and sea ice conditions. Increased amounts of sea ice may reduce the inaccuracies of the MWRP caused by neural network using radiosondes launched over land.

2.3 Data

The data were collected during the CFL project onboard the CCGS Amundsen from January until July 2008 and during the ArcticNet Cruise onboard the CCGS Amundsen from July until November 2009. A total of 68 profiles from radiosondes were used in the comparisons from both field campaigns. The radiosondes attached to a weather balloon when launched drift with the wind and deviate from the zenith as viewed by a MWRP. Thus, profiles were rejected if the RAOBS went out of range before reaching an altitude of 10 km or went in and out of range within the lower 10 km. The Vaisala RS92-SGPD radiosondes took 45 minutes to 1 hour for ascent. Furthermore, some launches occurred while the ship was in transit. To account for the drift of the balloons as well as the time for the balloon to ascend, the MWRP data was averaged over 1 hour starting at the time of launch, which allows for a comparable profile to the radiosondes. Fig. 2 shows the locations of the 68 comparable RAOB and MWRP profiles.

During CFL, an issue with the firmware installed on the base station for the radiosondes caused frequent drops in relative humidity readings. This impacted the absolute humidity values as they were calculated using the Clausius-Clapeyron equation from relative humidity. The firmware issue caused the relative humidity to rapidly decrease down to 10% or less and then rapidly increase back up. The relative humidity data were corrected using a linear interpolation. Data was rejected if erroneous relative humidity readings could not be distinguishable from natural decreases in relative humidity. As well, the entire radiosonde profile was rejected if either the rapid decreases and increases in relative humidity were very frequent, occurring for more than 40% of the time, or they occurred for longer than 90 seconds.

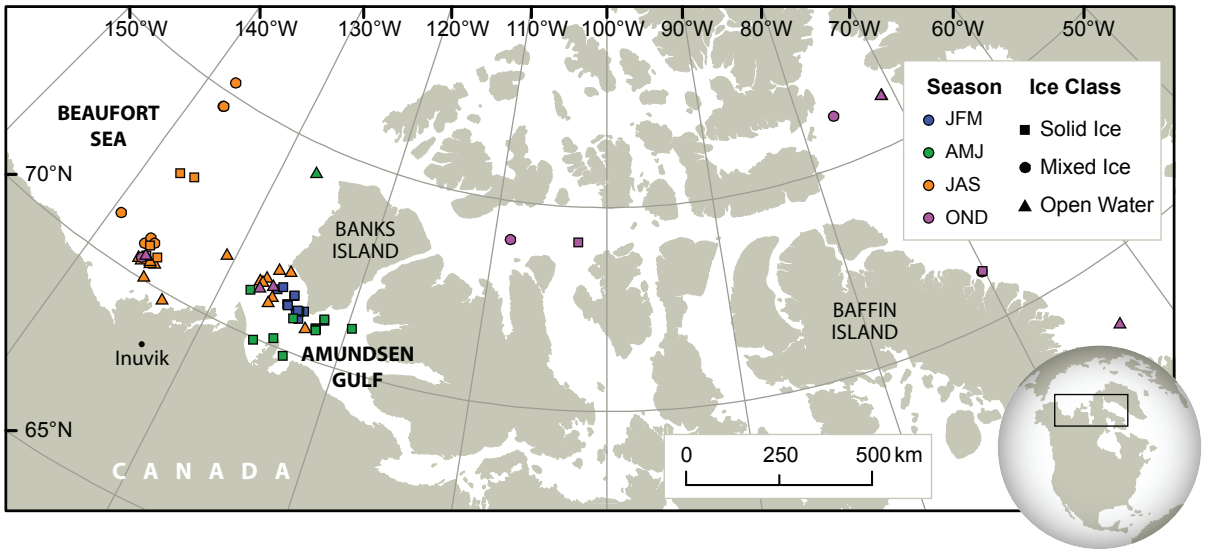

Figure 2: A map of the study region. Locations of the radiosonde profiles are shown, the colour represents the season it was launched: JFM - blue, AMJ - green, JAS - orange, OND - pink. The shape of the symbol represents the sea ice concentration class present at the time of the launch: solid ice - square, mixed ice - circle, open water - triangle.

The CCGS Amundsen is based out of Quebec City, Quebec, Canada. While travelling through the Northwest Passage to go to and from the Beaufort Sea, a total of 7 profiles were collected. Data collected in transit have been included in the data set, as the profiles were not outliers when the MWRP was compared to the RAOBS.

The atmospheric profiles were grouped by seasons with winter being defined as January, February and March (JFM), spring as April, May and June (AMJ), summer as July, August, and September (JAS) and fall as October, November, December (OND). The standard deviation of the RAOBS at each MWRP level was calculated for each season, Fig. 3. For JFM the temperatures measured by the RAOBS at the surface ranged from 240.5 K to 258.9 K with a mean temperature of 250.1 K and a standard deviation of 6.4 K. During JFM the surface temperatures were always well below freezing and the CCGS Amundsen, at the times of the radiosonde launches,

generally had thick first year ice in the immediate vicinity of the ship. 10 of the radiosondes were launched in areas where the ice thickness was greater than 1.0 m, 2 were in areas greater than 0.7 m and 2 profiles were taken during transit with the ice thickness unknown. In AMJ the surface temperatures measured by the RAOBS had a range of 248.1 to 273.0 K with a mean temperature of 264.0 K and a standard deviation of 7.7 K. In AMJ the surface temperatures reached the melting point of sea ice, which caused melt ponds to develop on the sea ice. JAS had a range from 269.4 to 290.2 K with the mean of 275.5 K and a standard deviation of 4.5 K. The sea ice concentration varied greatly during JAS, however with temperatures consistently above the freezing point mainly open water surrounded the ship. OND had surface temperatures ranging from 258.9 to 272.8 K with a mean of 265.2 K and a standard deviation of 4.8 K. For OND the temperatures dropped below the freezing point, resulting in new first year ice being formed. Due to the ship being in transit for part of this season, the sea ice concentration was greatly varied from open ocean $0/10^{ths}$ to consolidated $10/10^{ths}$ sea ice. With such a varied environment during the seasons, the RAOBS and MWRP profile data set covers a broad range of weather and surface conditions.

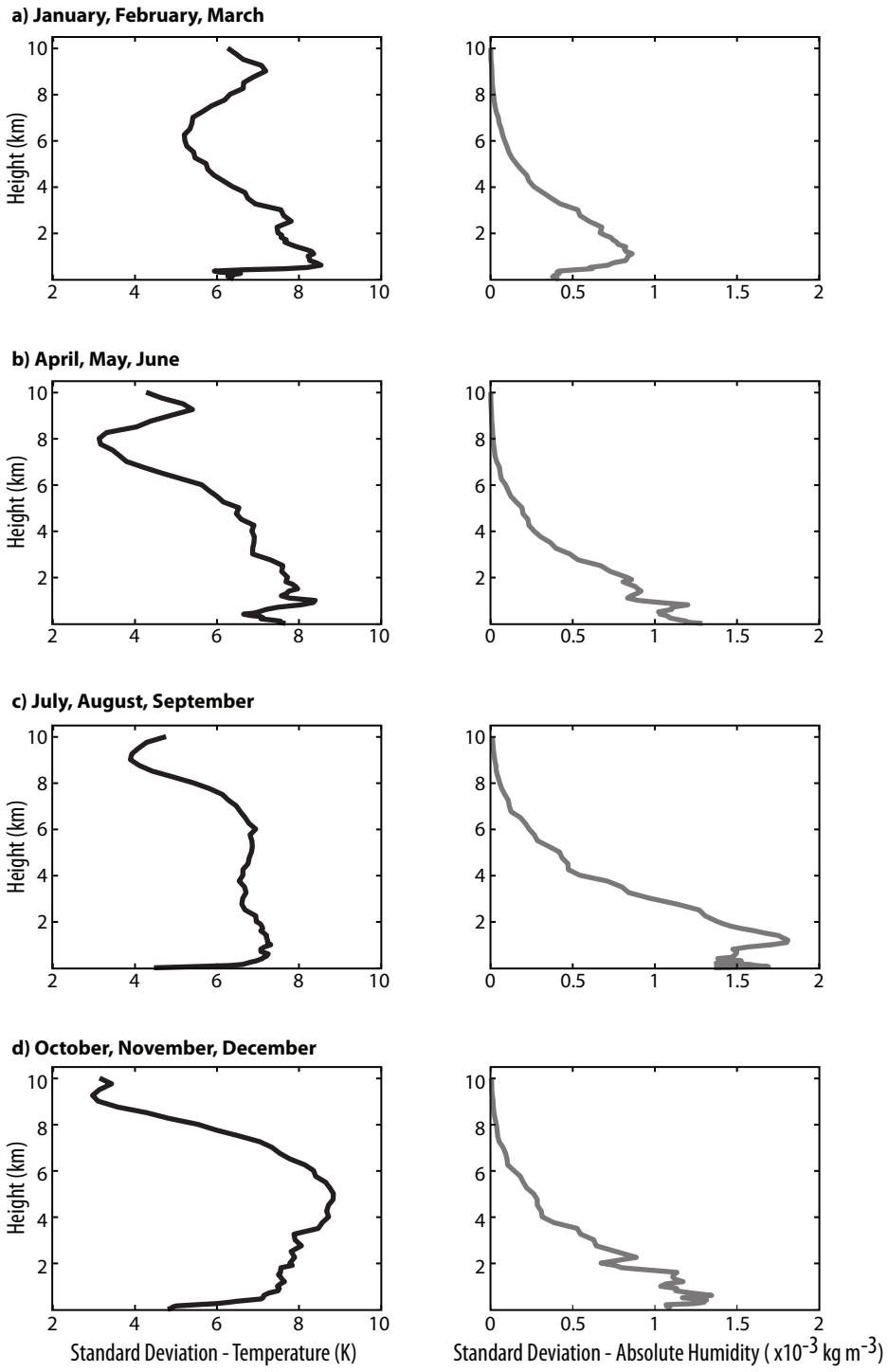

Figure 3: The standard deviation versus height in kilometers for temperature on the left and absolute humidity on the right. The standard deviation was calculated from the RAOBS used in the comparisons.

2.4 Validation with Radiosondes

The accuracy of a microwave profiling radiometer has been previously evaluated against radiosonde ascents over land. Guldner and Spankuch (2001) described radiosondes to be less than ideal references due to the ascending balloon travelling horizontally off-nadir and the inherent measurement errors in radiosondes, 0.5 K for temperature and 10% for relative humidity, makes them less than ideal references. The comparison is also difficult because the radiometric profiles are smoother than radiosonde soundings; the former observes a volume of air, while the latter provides a point measurement (Ware et al., 2003). Recently, Gaffard et al. (2008) reported that the accuracy of radiometer derived profiles for Linkenholt, UK decreased with height. RMS differences between radiosonde and radiometric measurements increased from 0.6 K near the surface to 1.5 K above 3 km for temperature, and from 0.5×10^{-3} kg m^{-3} near the surface to 1.1×10^{-3} kg m^{-3} between 1–2 km for water vapour. For Oklahoma and Kansas, USA, and for a location relatively close to the Cape Bathurst flaw lead polynya region, Barrow Alaska (71.30 °N; 156.78 °W), Liljegren et al. (2001) found RMS differences of 1–2 K for temperature. For water vapour, the RMS differences were 1–2 $\times 10^{-3}$ kg m^{-3} at the Great Plains sites, and 0.5×10^{-3} kg m^{-3} at Barrow where the average absolute humidity was small - about 1×10^{-3} kg m^{-3} near the surface.

There were a total of 14 comparable profiles for winter, 11 profiles for spring, 30 profiles for summer and 13 profiles for fall. Seasons can be artificial groupings in the Arctic with divisions based on a calendar date. Another stratification is sea ice concentrations which gives a better representation of the surface conditions present. To examine more closely the effect of sea ice and open water on the veracity of the

atmospheric boundary layer measured by the MWRP, the RAOB and MWRP profiles were also divided into three categories, regardless of season, based on the concentrations of sea ice surrounding the CCGS Amundsen. Open water was defined by $0/10^{ths}$ and $1/10^{th}$, mixed sea ice cover defined by $2/10^{ths}$ to $8/10^{ths}$ and very close pack or compact ice cover defined as $9/10^{ths}$ and $10/10^{ths}$. The sea ice concentrations were visual observations recorded by the ships officers or ice observers and were subjective. As the visual horizon is about 25 km, these observations represent the sea ice concentrations within 25 km of the CCGS Amundsen. By dividing the data into only three sea ice concentration categories the subjectivity was reduced since $2/10^{ths}$ to $8/10^{ths}$ are the most open to interpretation and are grouped together into one category. Poor visibility also caused a problem for observing ice cover. Fog and poor visibility occurred during times when no radiosondes were launched and no data were discarded due to this limitation.

The mean atmospheric profile, as measured by the radiosondes, was calculated for each season, Fig. 4, and sea ice concentration group, Fig. 5. The mean temperature profile for JFM shows a strong temperature inversion with a lapse rate of 5.0 K km^{-1} in the bottom 1 km, Fig. 4a. During JFM the sea ice concentrations at the time of the RAOBS were either $9/10\ ^{ths}$ or $10/10^{ths}$. When the data was grouped by sea ice concentrations the average profile for consolidated ice, $9/10\ ^{ths}$ or $10/10^{ths}$, showed only a very weak temperature inversion with a lapse rate of 2.1 K km^{-1}, Fig. 5a. The consolidated ice category includes profiles that were taken during each of the four seasons, which caused the differences from JFM in the mean temperature and humidity profiles. The average surface temperature during JFM is 10 K less than the average surface temperature of the consolidated ice category. The mean absolute humidity during JFM is less than 1×10^{-3} kg m^{-3} from the surface up to 2 km, where as for consolidated ice the mean absolute humidity is 2×10^{-3} kg m^{-3} at the surface

and reduces to 1.5 $\times$ 10^{-3} kg m^{-3} at 2 km. The mixed ice category has 7 profiles during JAS and 4 from OND. As a result, the mean temperature profile for mixed ice is approximately 5 K warmer than OND and 5 K cooler than JAS. Similarly, the mean humidity profile for mixed ice has less moisture at the surface than JAS and more moisture than OND. The open water group, 0/10 ^{ths} or $1/10^{th}$, consists of 18 profiles during JAS, with 1 profile in AMJ, and 7 from OND. The resulting mean temperature profile is slightly cooler than JAS, similarly the mean absolute humidity profile is slightly drier.

The root-mean-square (RMS) difference and bias were calculated for each of the MWRP levels and grouped by season, Fig. 6. The RMS difference and biases were calculated as the RAOBS minus the MWRP. The RMS difference and bias profiles for temperature, left hand column Fig. 6, shows that the RMS difference and bias drastically increase with height above 4 km. For JFM, the RMS difference at 4 km is 2.37 K with an average of 1.92 K for the bottom 4 km. From the height of 4 km, the RMS difference increases to 6.20 K at 10 km. Similarly, AMJ has an average RMS difference of 1.95 K below 4 km, and a RMS difference of 1.65 K at 4 km, which increases to a maximum of 5.64 K at 9.5 km. For JAS, the lower 4 km has a higher average RMS difference of 2.76 K with 3.47 K at 4 km. The RMS difference increases only to 4.93 K at 6 km and remains above 4 K up to 10 km. OND has an average value of 2.46 K for the lower 4 km and drastically increases from 4 km to 6 km with a maximum value of 5.07 K. The RMS difference then decreases to 3.29 K at 10 km. Each season shows, on average, a moderate increase with height in the RMS difference below 4 km. Below 4 km the RMS and bias show a difference of 3 K or less, except for JAS, which is 4 K or less. For all seasons the rate of increase for the RMS difference, above 4 km, was drastic. This indicated that the MWRP data above 4km should be viewed with skepticism.

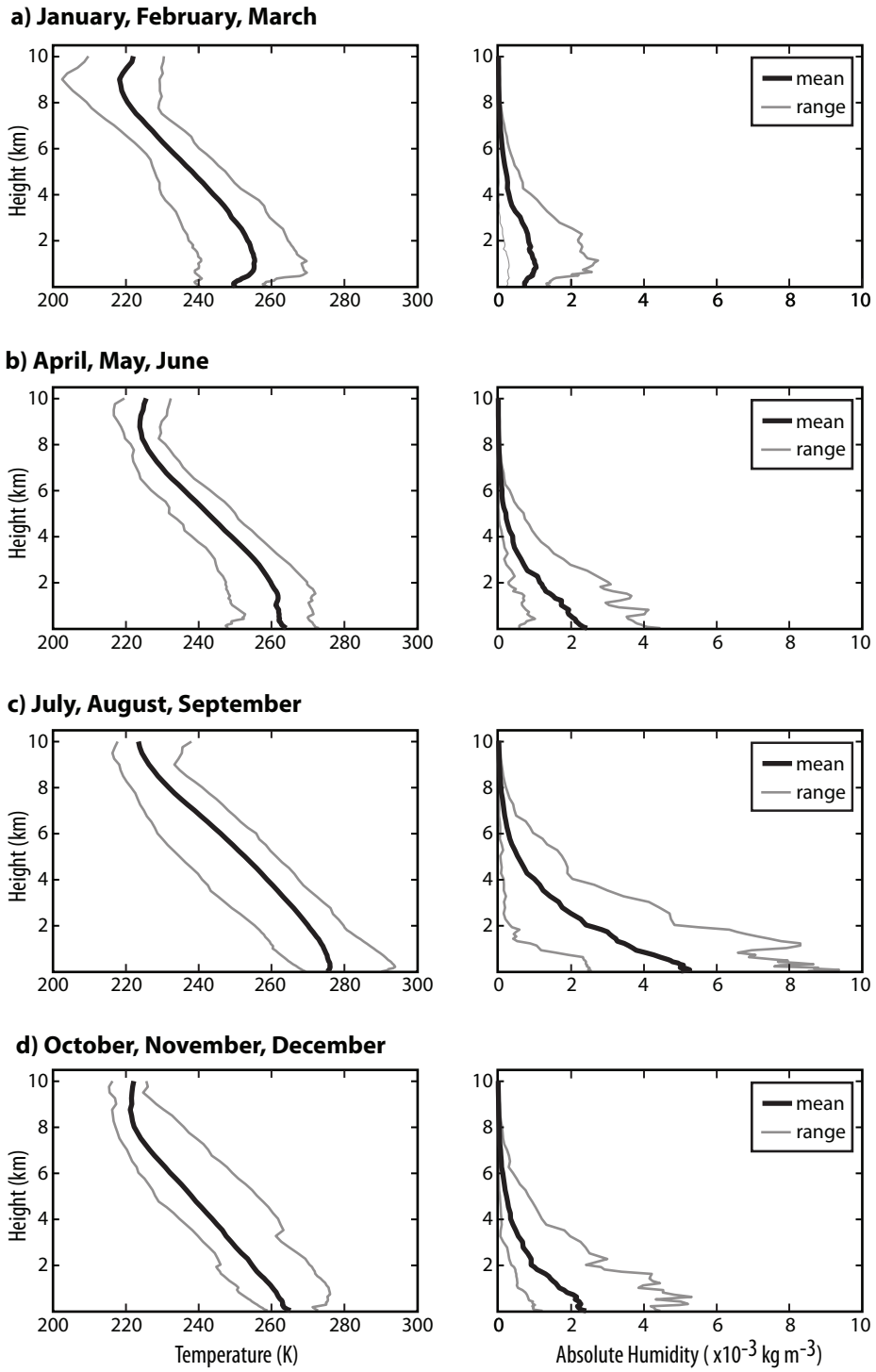

Figure 4: The mean atmospheric profile versus height in kilometers for temperature on the left and absolute humidity on the right. The mean was calculated from the RAOBS used in the comparisons. The data were categorized by seasons (JFM, AMJ, JAS and OND).

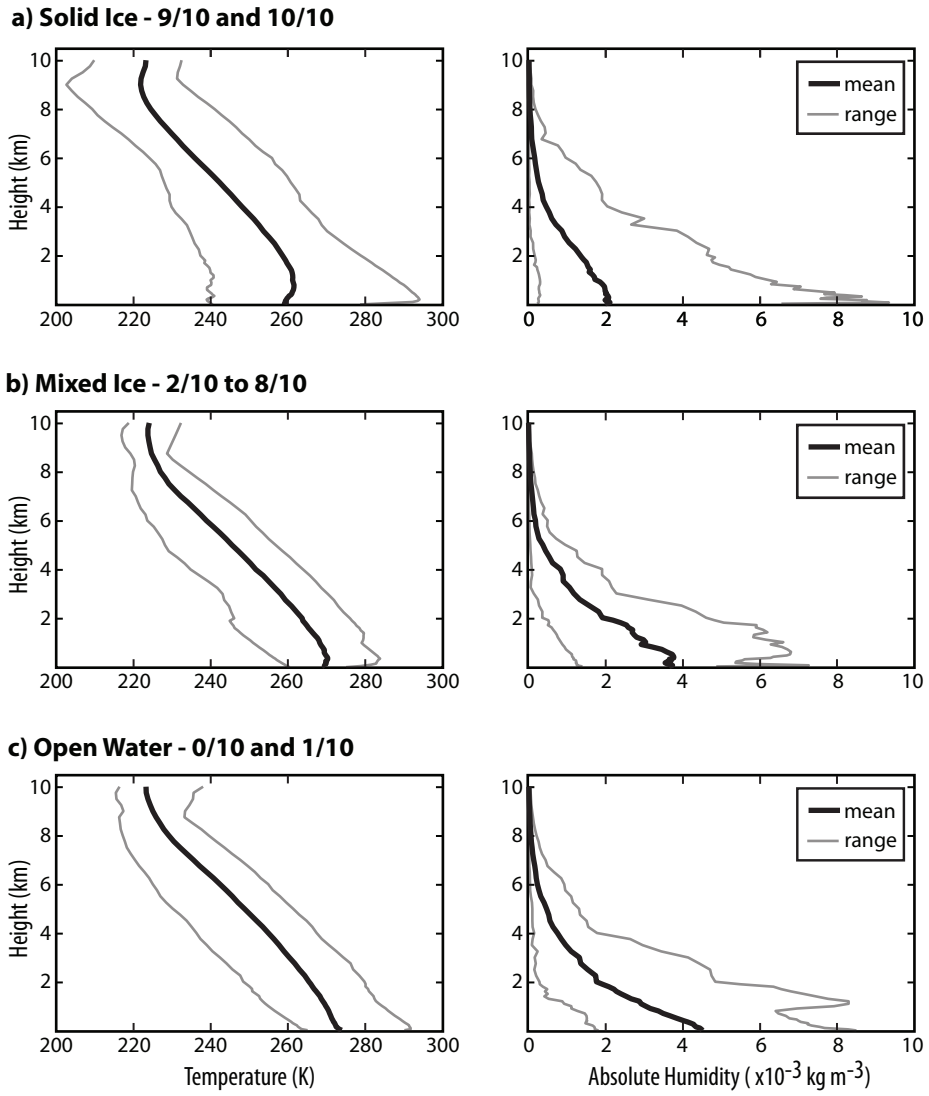

Figure 5: The mean atmospheric profile versus height in kilometers for temperature on the left and absolute humidity on the right. The mean was calculated from the RAOBS used in the comparisons. The data were categorized by sea ice concentrations.

The right column, Fig. 6, is the RMS difference and bias profiles for the absolute humidity for each season. The absolute humidity has a much smaller RMS difference in winter than in any other season; this is to be expected due to the very low absolute humidity values that are characteristic of the dry winter climate in the high Arctic.

The RMS and bias profiles, for the three sea ice concentration categories for 0 to 2 km are given, Fig. 7. These RMS and bias calculations are restricted to the lowest 2 km as the characteristics of the surface should only impact the atmospheric boundary layer and not the entire profile (Overland and Guest, 1991).

The RMS and bias for absolute humidity over solid ice is generally smaller than over mixed ice or open water, Fig. 7, right column. The RMS for absolute humidity over solid ice stays around 0.5 $\times$ 10^{-3} kg m^{-3}, where as over mixed ice the RMS is much more varied and has a range from 0.25 to 1.0 $\times$ 10^{-3} kg m^{-3} in the lower 2 km. Over open ocean the absolute humidity is less varied than over mixed ice, but is still generally larger than over solid ice, with a range from approximately 0.5 to 0.75 $\times$ 10^{-3} kg m^{-3}. The RMS and bias for absolute humidity is of an order of magnitude smaller than the RMS and bias for temperature, which is the same as when categorized by season.

When the RMS and bias profiles are categorized by sea ice concentration the mean temperature biases are consistently positive for all sea ice groups with a small exception near the surface, Fig. 7, left column. When there is very little open water, $9/10^{ths}$ or $10/10^{ths}$ sea ice concentration, the mean RMS and bias stays below 3 K. For both open water and mixed sea ice concentrations the RMS and bias remains below 4 K up to 2 km in height. There is not a significant difference between the RMS and bias for open water, mixed sea ice and for solid ice, below 2 km, when

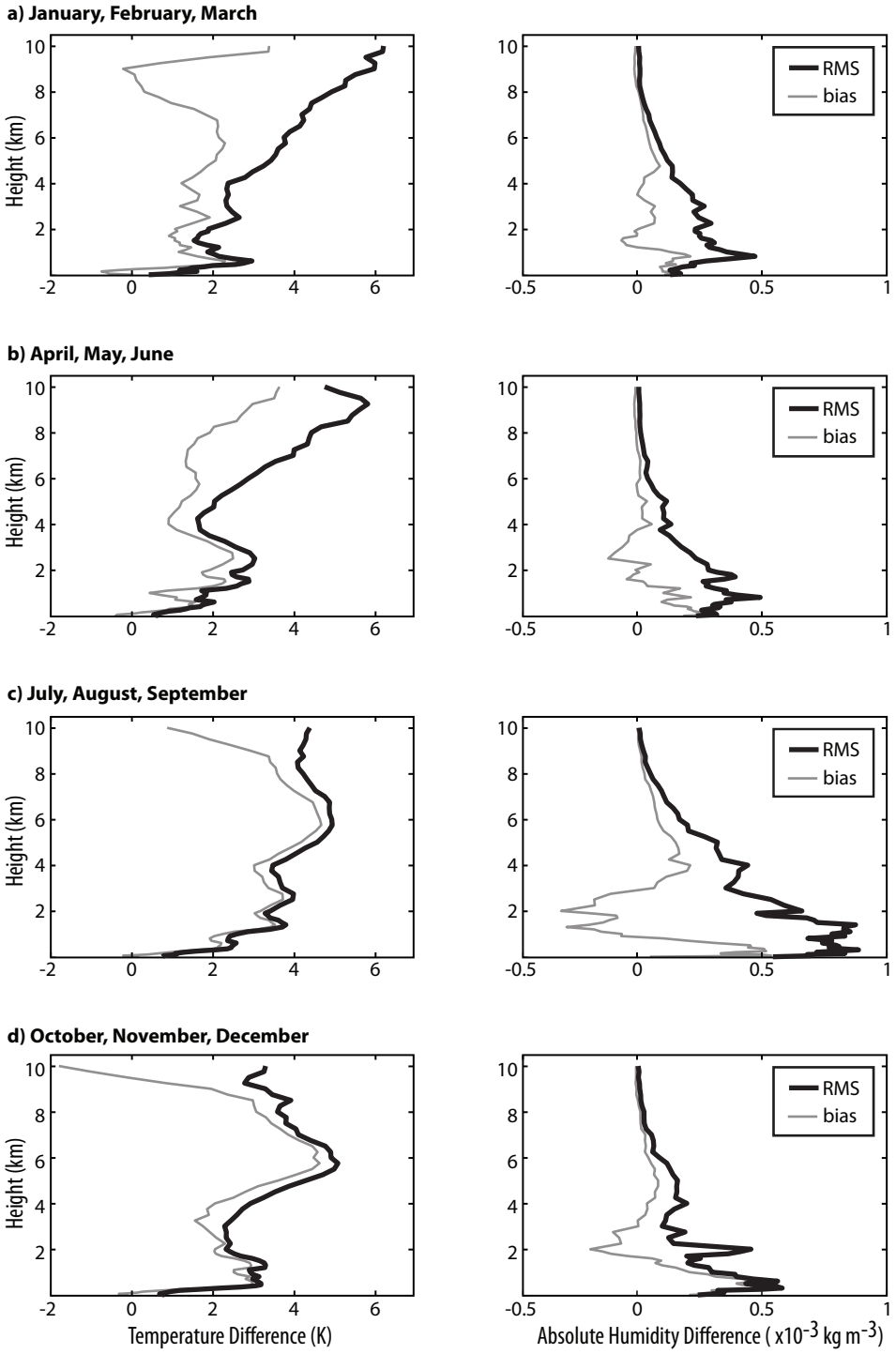

Figure 6: The root-mean-square difference, and bias versus height in kilometers for temperature profiles on the left and absolute humidity on the right, from Vaisala RS92-SGP radiosondes and Radiometrics microwave profiling radiometer. The bias was determined by the RAOBS minus the MWRP.

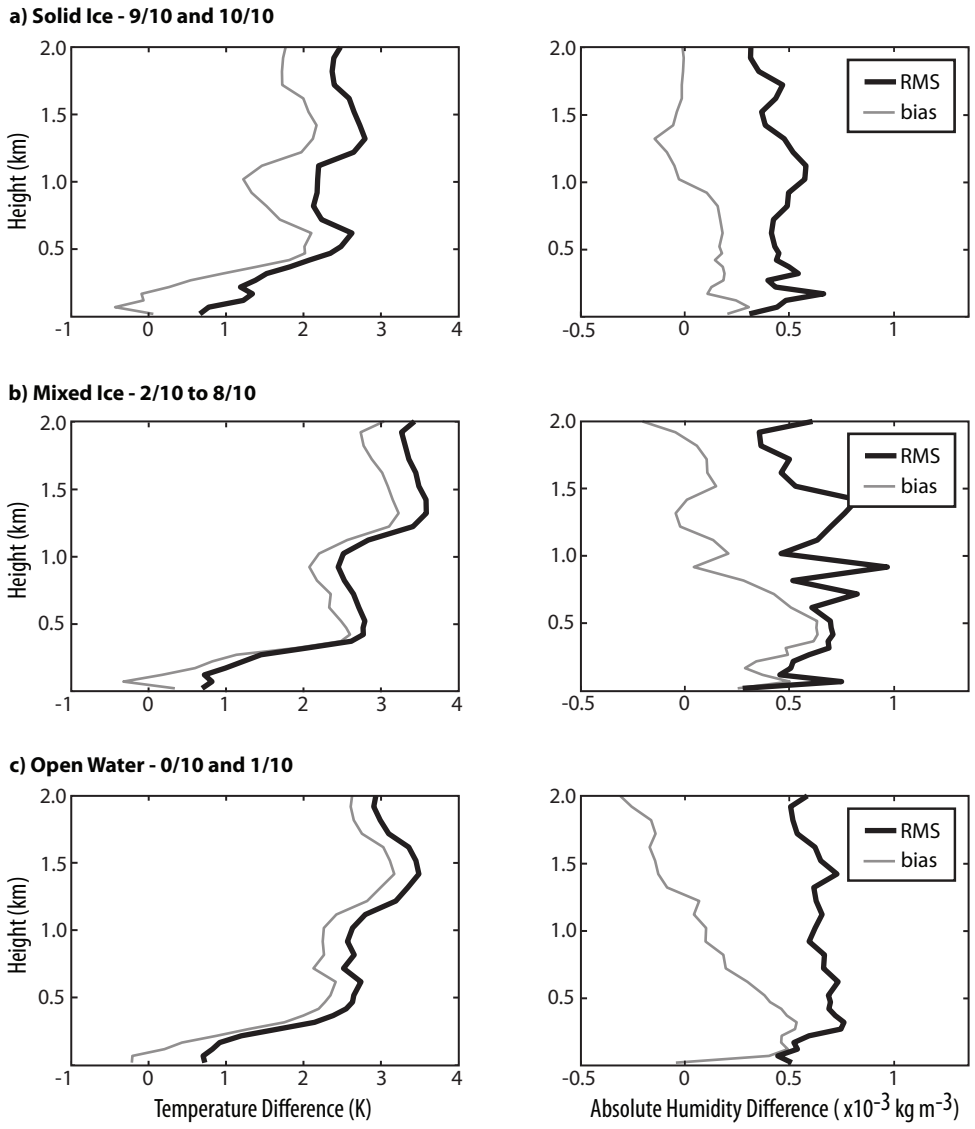

Figure 7: The root-mean-square difference, and bias versus height in kilometers for temperature profiles on the left and absolute humidity on the right. The data were categorized by sea ice concentration. The bias was determined by the RAOBS minus the MWRP.

compared to the seasonal data. The RMS differences when compared to the other validation studies indicate that the MWRP can reliably measure the boundary layer over varied sea ice concentrations.

The frequency distribution of the bias was plotted, Fig. 8. The bias, RAOBS minus MWRP, was calculated for each of the 68 atmospheric profiles. The data were grouped into 5 classes with heights of a) 0 – 0.1 km, b) 0.4 – 0.5 km, c) 0.9 – 1.1 km, d) 4.75 – 5.25 km and e) 9.5 – 10 km. Each height class contains 204 bias measurements. For both temperature and absolute humidity, the data were divided into class intervals with a width 0.5, where -0.25 to 0.25 is defined as the 0 interval. If the sample was large enough and the errors were random, the frequency distributions would be normal and centered on zero. Looking at the temperature distribution, left column Fig. 8, all height levels exhibit an obvious positive skewness, with the exception of the 9.5 to 10 km level. The 9.5 to 10 km level does have a positive skewness although the distribution curve is multimodal rather than a normal curve. The absolute humidity distribution, right column Fig. 8, also shows an obvious positive skewness, with every height level clearly centered with a positive bias. Having a relatively large sample of 204 measurements and generally a positive skewed distribution indicates that the errors are systematic. The temperature distribution with a positive skewness indicates that the MWRP has a systematic cold bias compared to the RAOBS. Similarly, the positive skewness for the absolute humidity indicates that the MWRP has a systematic dry bias compared to the RAOBS. This could be due to the MWRP having a neural network that was trained with data from land-based radiosondes. The MWRP profiles may exhibit a dry bias more akin to the climate conditions found at Inuvik, rather than a marine climate.

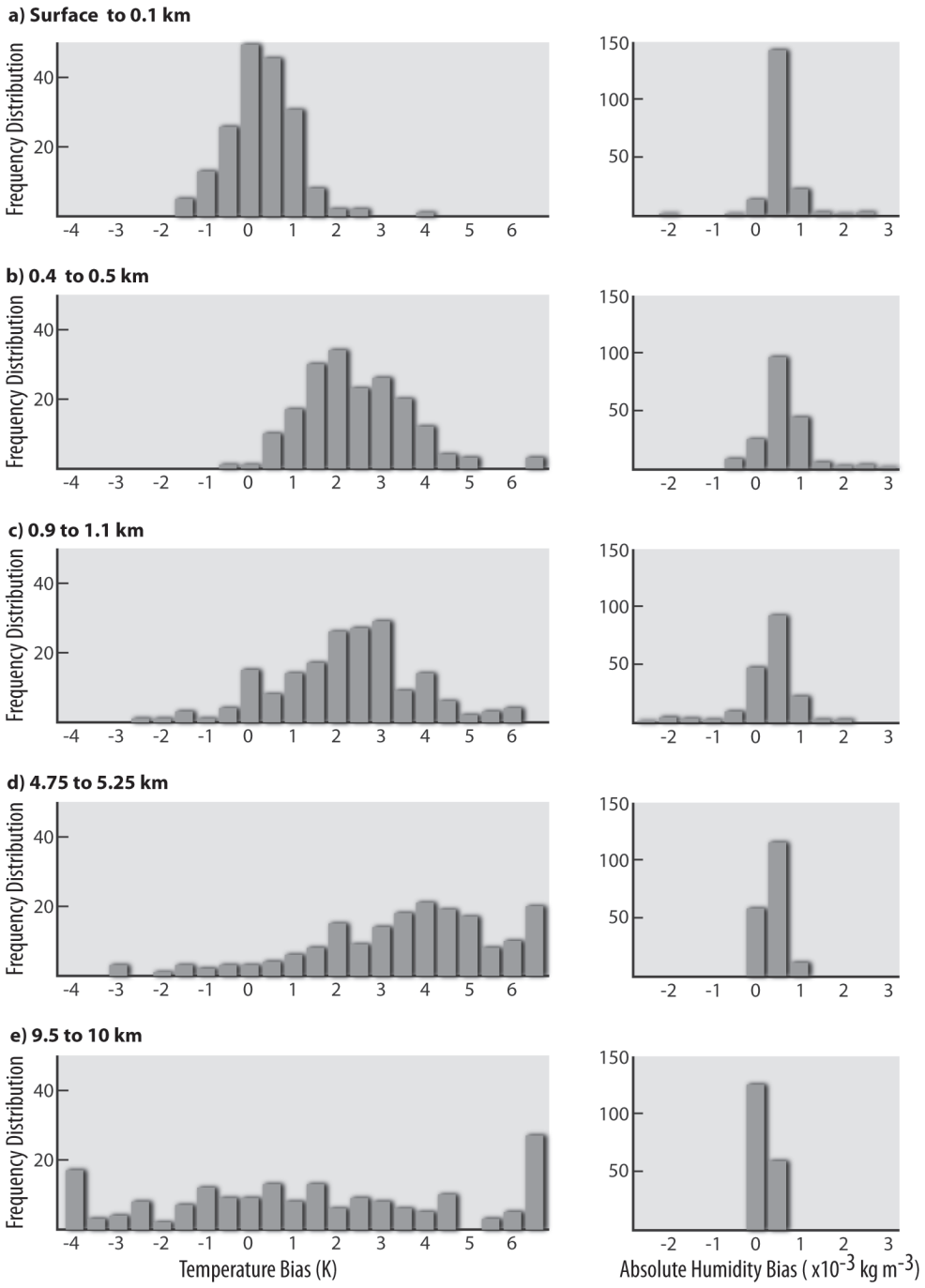

Figure 8: The frequency distribution of the MWRP bias. The data were grouped by heights, a) 0 – 0.1 km, b) 0.4 – 0.5 km, c) 0.9 – 1.1 km, d) 4.75 – 5.25 km and e) 9.5 – 10.0 km. The bias was calculated as the RAOBS minus the MWRP.

2.5 Case Study

From 25 July 2009 at 1245 until 27 July 2009 at 1200, five radiosondes were launched at intervals of 10 to 14 hours. These 5 profiles create a time series in which a warm front moved into the area. Since the measurements from both the RAOBS and MWRP are taken onboard a ship that was mobile, the captured warm front is not geo-spatially accurate. During the passage of this warm front, the surface temperatures increased from 0.6 °C at 1200 UTC, 25 July to a maximum recorded surface temperature of 5.3 °C at 0300 UTC, 27 July. No precipitation was recorded during the event, however the recorded cloud cover ranged from $0/8^{ths}$ to $8/8^{ths}$. With the warm front a surface inversion was present; the inversion had a difference of 15 °C between the surface and approximately 1 km , which later strengthened to 21 °C. Temperature and humidity inversions are dominant features during the Arctic winter, inversions occurring in the summer tend to occur less often and are generally weaker (Overland, 2009).

Fig. 9 and 10 show the temperature and absolute humidity profiles during the 48 hour time period starting on 25 July 2009 at 1245 UTC. Fig. 9a shows the temperature as interpreted from the 5 radiosonde profiles. Intermediate temperature values were calculated using a cubic spline interpolation at intervals of 28.8 minutes at every height level given by the MWRP. Fig. 9b shows the raw data from the MWRP using the data with the nearest time to the 28.8 minute interval. Fig. 9c shows the difference between the two, the RAOBS minus the MWRP. Fig. 10, was calculated in the same manner as Fig. 9 except for absolute humidity rather than temperature.

Initially there is an apparent similarity between the RAOBS and MWRP temperature

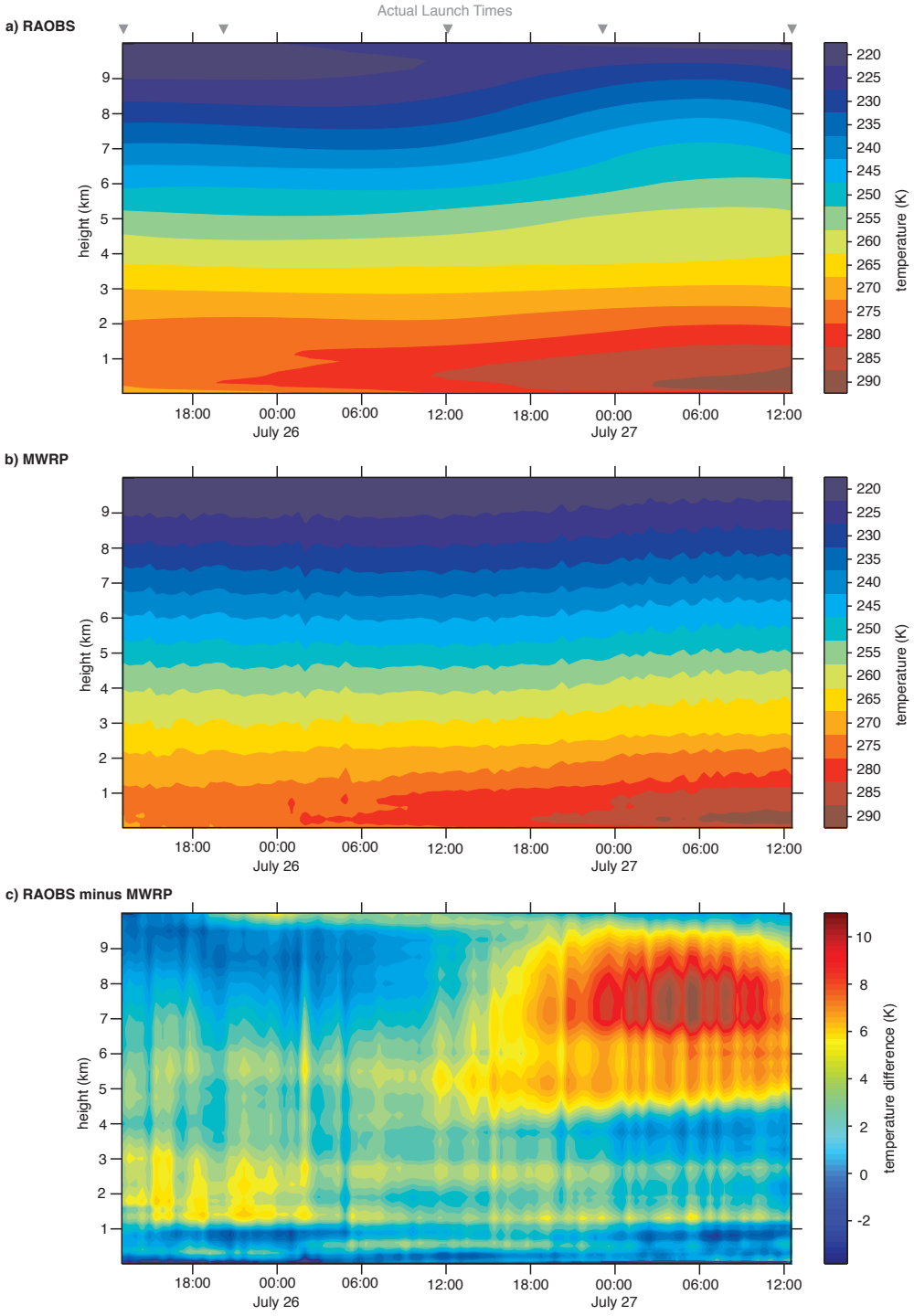

Figure 9: The radiosonde temperature data from 5 launches was calculated using a cubic spline interpolation over the period from 25 July 2009 at 1245 UTC until 27 July 2009 at 1247 UTC as shown in 6a. 6b shows the raw MWRP data from that same time period while 6c shows the difference between the two, RAOBS minus MWRP.

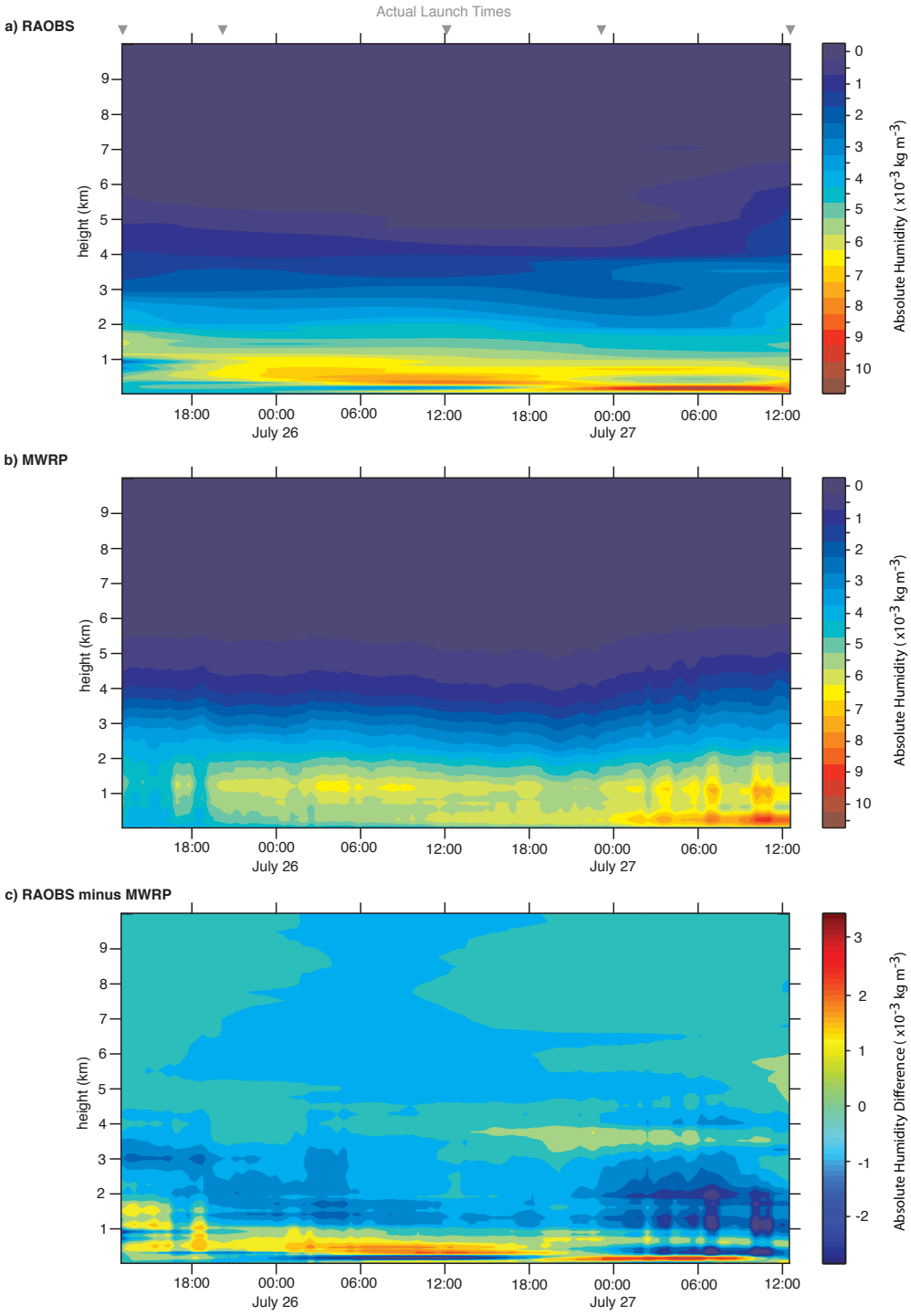

Figure 10: Same as figure 6 except for absolute humidity.

measurements, Fig. 9. The measurements below 2 km agree well, however there is a discrepancy between the two starting at approximately 26 July 2009 at 1800, where the RAOBS minus the MWRP have a large difference in temperature at heights above 5 km. A similar, but much more subtle difference in absolute humidity is also noted for the same altitude and time frame, Fig. 10. This difference may be due to a discrepancy in the accuracy of the MWRP to resolve the modification of absolute humidity and temperature profiles by forced lift along an advancing front. During the passage of the warm front, Fig. 9 and 10, warmer less-dense air from behind the front was forced to ascend over the cooler, denser air ahead of the front. Images from the all-sky camera mounted onboard the CCGS Amundsen show cumulus clouds over the area from about 01:00 – 12:00 27 July. The ceilometer data indicates that the cloud height ranged from 1000 to 1700 m during the same time. Moisture was simultaneously forced vertically, and is evident in the development of a moisture plume at the 2 – 3 km altitude range, Fig. 10. The plume builds in magnitude most notably from 00:00 - 12:00 27 July, where the absolute humidity increased on average by 0.68 g m^{-3}, from the previous 12 hours, and corresponded with the large difference between the MWRP and RAOBS measurements.

Looking at Fig. 10, there is again a similarity between the RAOBS measurements for absolute humidity and the MWRP measurements. Fig. 10c shows there is very little difference between the RAOBS and the MWRP measurements above 5 km; this is not surprising as the humidity drops to near zero. The MWRP shows the increase in moisture from the warm front, however there are differences between the RAOBS and the MWRP near the surface. This may be due to the MWRP being trained with profiles from Inuvik, which is over land rather than over the ocean where the MWRP is actually being used.

2.6 Vertical Resolution

Vertical resolution defined by Smith et al. (1999) is given by the half width of the inter-level covariance matrix, equation (1). Both Smith et al. (1999) and Guldner and Spankuch (2001) suggest, this method gives the lower limit of the vertical resolution. Through case studies, Guldner and Spankuch (2001) show that the MWRP has a higher vertical resolution than the inter-level covariance method suggests.

$$C(z_0, z) = \frac{\sum_{i=1}^{N}[T_r(z_0) - T(z_0)][T_r(z) - T(z)]}{\sqrt{\sum_{i=1}^{N}[T_r(z_0) - T(z_0)]^2 \sum_{i=1}^{N}[T_r(z) - T(z)]^2}}. \quad (1)$$

Equation 1 gives the vertical inter-level covariance for temperature. Where N is the number of MWR and RAOB profile comparisons, T_r is the temperature from the MWRP, T is the temperature from the RAOBS. z is the height and z_0 is the reference height for which the vertical resolution is being defined. Vertical resolution is defined as the half-width of the covariance function for each measured height.

The vertical resolution for temperature had a skewed error covariance, which affected the estimate of the vertical resolution. This may be due to the vertical resolution being calculated with only 68 profiles, collected over a two year time period. Before calculating the vertical resolution, the average bias for each height level was removed from the MWRP data based on sea ice concentration, as the method defined by Smith et al. (1999) requires. Fig. 11 shows the vertical resolution of temperature and absolute humidity of the MWR profiles for up to 8 km in height.

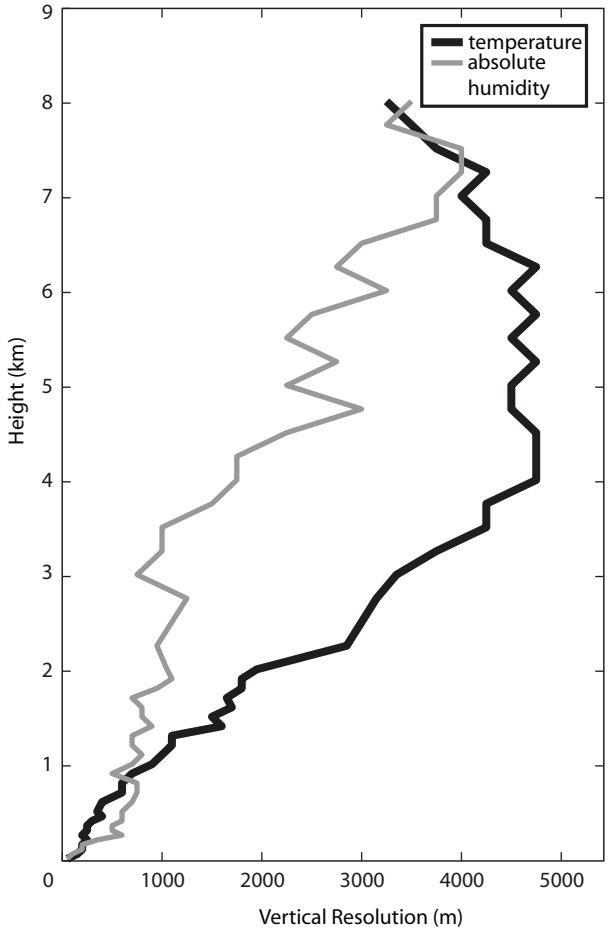

Figure 11: The vertical resolution of the MWRP in meters against height in kilometers as calculated by the inter-level covariance method.

As shown in Fig. 11, the lower limit of the resolution degrades more slowly for the absolute humidity than for temperature. The vertical resolution for temperature degrades substantially above 1.5 km to a minimum value of 4750 m at 4 km then increases to 3250 m at 8 km. The vertical resolution for absolute humidity stays below 1000 m up to 2 km, and there is a significant degradation from 1000 m to 3000 m in the resolution between approximately 3.5 km and 5 km.

As suggested by Smith et al. (1999) and Guldner and Spankuch (2001), the inter-level covariance method of calculating the vertical resolution is a lower limit. The previous statistical analyses of the data and the case study lead to the conclusion that the vertical resolution of the MWRP is much greater than that indicated by the inter-level covariance method.

2.7 Discussion and Conclusion

A total of 68 radiosonde profiles were used to verify corresponding radiometer profiles. The 68 profiles were grouped by season and underlying sea ice concentrations. There appears to be a larger bias for both temperature and absolute humidity when there are low concentrations of sea ice present. Higher concentrations of sea ice act as a barrier reducing the transfer of heat and moisture between the ocean and the atmosphere (Barry et al., 1993), therefore lower concentrations of sea ice may result in more moisture in the Arctic marine atmosphere. The larger bias with low concentrations of sea ice is not unexpected as the MWRP employs a neural network that is trained using historical radiosondes launches. Due to the limited spatial and temporal radiosonde history in this region, radiosonde data from Inuvik, NWT, Canada is employed. This may have introduced a bias close to the surface in the neural network coefficients, and may have lead the MWRP to exhibit a dry bias, akin to the climate conditions found at Inuvik, rather than a marine climate.

RMS differences for temperature (RAOBS - MWRP) averaged 1.79 K through the lowest 2 km for the winter (JFM) season, 1.81 K for the spring (AMJ) season, 2.51 K for the summer (JAS) season, and 2.47 K for the fall (OND) season. Average biases of +0.99 K, +1.19 K , +2.13 K , and +2.08 K , respectively, indicating that the MWRP measurements were colder than the RAOBS for the lower 2 km. Similarly biases for the upper 2 to 8 km and 8 to 10 km were all positive, again indicate that the MWRP consistently recorded lower temperatures than the RAOBS.

The RMS difference for absolute humidity (RAOBS - MWRP) averaged 0.25×10^{-3} kg m^{-3} in the lowest 2 km during the winter (JFM) season, 0.32×10^{-3} kg m^{-3} for

the spring (AMJ) season, 0.14×10^{-3} kg m^{-3} for the summer (JAS) season, and 0.23×10^{-3} kg m^{-3} for the fall (OND) season. Average biases of $+0.08 \times 10^{-3}$ kg m^{-3} for profiles over $9/10^{ths}$ and $10/10^{ths}$ sea ice concentration, $+0.26 \times 10^{-3}$ kg m^{-3} for profiles over mixed sea ice concentrations ($2/10^{ths}$ to $8/10^{ths}$), and $+0.16 \times 10^{-3}$ kg m^{-3} for over open water ($0/10^{ths}$ and $1/10^{th}$), indicated that the MWRP measurements were slightly drier than the RAOBS for the lower 2 km. The sea ice concentrations of $9/10^{ths}$ and $10/10^{ths}$ have the lowest bias, which is to be expected with the least amount of open water present.

The vertical resolution was calculated using the inter-level covariance method as defined by Smith et al. (1999). The vertical resolutions calculated were in general as coarse as the height measured; at a height of 1 km the vertical resolution was approximately 1000 m. This could be a result of the data set being limited to a total of 68 profiles and the resulting covariance curves being very skewed rather than bell shaped. Although currently this is the only method available, we conclude that the resolutions given are far too coarse compared to the resolution suggested by the statistical analysis of the individual seasons and as shown in the case study. Future work should involve the development of a new method for calculating the vertical resolution of the MWRP.

The objective of this paper was to determine how reliable the MWRP is when mounted onboard a mobile ship in the high Arctic. Although the MWRP had difficulty with forced lift along an advancing front and with near surface humidity, as seen in the case study, the data retrieved from the MWRP are still suitable for profiling lower level boundary layer weather and climate. Based on the comparison of the MWRP with the RAOBS and the case study we conclude that the MWRP does give reliable measurements of both temperature and absolute humidity.

Acknowledgments

This work was funded by the Natural Sciences and Engineering Research Council (NSERC), the International Polar Year (IPY) Federal Program Office, and the Canada Research Chairs (CRC) programs through grants to D.G.Barber. Thanks to C.R. Candlish, A.C. Coates and R. Scharien for their contributions. We would like to acknowledge the tireless efforts of the crew and captain of the CCGS Amundsen.

References

Barber, D. G., Asplin, M., Gratton, Y., Lukovich, J., Galley, R., Raddatz, R., and Leitch, D. (2010). The international polar year (ipy) circumpolar flaw lead (cfl) system study: introduction and physical system. *Atmos.- Ocean*.

Barry, R., Serreze, M., Maslanik, J., and Preller, R. (1993). The arctic sea ice-climate system: Observations and modeling. *Reviews of Geophys.*, 31(4):397.

Gaffard, C., Nash, J., Walker, E., Hewison, T. J., Jones, J., and EG, E. G. N. (2008). High time resolution boundary layer description using combined remote sensing instruments. *Ann. Geophys.*, 26:2597–2612.

Guldner, J. and Spankuch, D. (2001). Remote sensing of the thermodynamic state of the atmospheric boundary layer by ground-based microwave radiometry. *J. Atmos. and Oceanic Tech.*, 18:925–933.

Liljegren, J., Lesht, B., Kato, S., and Clothiaux, E. (2001). Initial evaluation of profiles of temperature, water vapor and cloud liquid water from a new microwave profiling radiometer. In *Proceedings of the 5th Symposium on Integrated Observing Systems*.

Maykut, G. (1978). Energy exchange over young sea ice in the central arctic. *Journal of Geophysical Research*, 83(C7):3646–3658.

Overland, J. E. (2009). Meteorology of the beaufort sea. *J. Geophys. Res*, 114.

Overland, J. E. and Guest, P. S. (1991). The arctic snow and air temperature budget over sea ice during winter. *J. Geophys. Res*, 96:4651–4662.

Smith, W. L., Feltz, W. F., and and, R. O. K. (1999). The retrieval of planetary boundary layer structure using ground-based infrared spectral radiance measurements. *J. Atmos. and Oceanic Tech.*, 16:323–333.

Solheim, F., Godwin, J. R., Westwater, E. R., Han, Y., Keihm, S. J., March, K., and Ware, R. (1998). Radiometric profiling of temperature, water vapor, and cloud liquid water using various inversion methods. *Radio Science*, 33:393–404.

Ware, R., Carpender, R., Guldner, J., Liljegren, J., Nehrkorn, T., Solhelm, F., and Vandenberghe, F. (2003). A multichannel profiler of temperature, humidity, and cloud liquid. *Radio Science*, 38:1–44.

On the Use of CloudSat and Calipso to Study Clouds in a High Latitude Polar Environment

Lauren M. Candlish

Richard L. Raddatz, Matthew G. Asplin and David G. Barber

Prepared for the Journal of Geophysical Research - Atmopshere

April 5, 2011

3 On the Use of CloudSat and Calipso to Study Clouds in a High Latitude Polar Environment

In the previous chapter, the veracity of a Radiometrics microwave profiler was investigated. Data was used from the MWRP to compare against satellite data. This chapter is a paper prepared for publication to the Journal of Geophysical Research - Atmosphere as part of the CFL special edition. The manuscript is a validation of the satellites CloudSat and Calipso's data products ECMWF-aux and GeoProf-lidar. It statistically compares temperature and humidity measurements from a Radiometrics microwave profiling radiometer and the ECMWF-aux data product. Cloud base height as measured by both the MWRP and the ceilometer is compared to the cloud base height from the GeoProf-lidar data product. The co-author's are Rick Raddatz, Matt Asplin and David Barber. Rick Raddatz was involved in the editing of the manuscript. Matt Asplin helped with the collection of the field data and post processing of the raw MWRP data, as well as editing the manuscript. David Barber provided funding for this research, contributed to ideas through his supervisory role, and contributed edits to the manuscript.

3.1 Introduction

Clouds play a major role in the Arctic's energy budget (Curry et al., 1996). Thus, they are a critical part of the Arctic climate system. Clouds exert a profound influence on the solar radiation that enters and the longwave radiation that leaves the atmosphere (Curry et al., 1996; Walsh and Chapman, 1998; Minnett, 1999). The cloud-radiation feedback mechanism in the Arctic is described by Curry et al. (1996). Cloud properties, such as cloud fraction and cloud optical depth have direct impacts on the net radiation which, in turn, affects the surface temperatures and sea ice cover. During winter, clouds warm the surface by decreasing the loss of longwave radiation to space. Thus, a decrease in cloudiness leads to a cooler surface temperature, and an increase in sea ice cover and vise versa (Schweiger, 2004). A change in sea ice fraction can affect the surface sensible and latent heat fluxes. Changes in surface sensible and latent heat fluxes affect the temperature and humidity of the atmospheric boundary layer. Changes in temperature and humidity then have a feedback affect on the cloud fraction and cloud optical depth. Thus, it is evident that accurate cloud observations are essential to the understanding and simulation of the Arctic climate system.

Curry et al. (1996) also describes an escalating sea ice-albedo feedback mechanism in the Arctic due to climate change. As the atmosphere warms, snow and ice cover will decrease, leading to a decrease in surface albedo and an increase in the absorption of solar radiation at the surface, which will lead to further warming. Similarly, if the climate cools, ice cover will increase, which increases the albedo and thus decreases the absorption of solar radiation at the surface, which favours further cooling. This scenario would be disrupted if warming is accompanied by increased cloud cover.

Visual observations and classifications of clouds during winter in the Arctic are hindered by the lack of illuminating sunlight (Hahn et al., 1995). Ambiguities in cloud classification have also contributed to the lack of accuracy in observing and reporting (Curry et al.,

1996). Low-level ice crystal clouds, also referred to as clear-sky ice crystal precipitation or "diamond dust", are often unreported or misclassified. The ice crystal particles impact the radiation budget and thus accurate observing and reporting of them is useful for the interpretation of satellite remote sensing and for climate modeling studies (Curry et al., 1996).

Several cloud climatologies have shown that at high latitudes clouds cover most of the sky and the dominant low-level clouds are stratocumulus (Curry et al., 1996). Isaac and Stuart (1996) have shown that the most common precipitating cloud in the Mackenzie River Valley - Beaufort Sea area is stratocumulus. Jin et al. (2007) report that high clouds appeared more frequently in winter than in spring during the Canadian Arctic Shelf Exchange Study (CASES) over wintering experiment. However, they suspect that this could be due to observers and instruments being unable to see beyond the low- and mid-level clouds that are common in spring and summer. Seasonally spring and summer are cloudier periods in the Arctic with the maximum total cloud cover increasing to 90% during summer (Curry et al., 1996), when low-level stratiform clouds are a dominant feature in the Arctic (Tsay et al., 1989). The cloud cover minimum occurs during winter with values ranging from 40% to 68% (Curry et al., 1996).

Schweiger (2004) showed that there has been a marked increase in cloudiness in the Arctic over the past two decades based on the TOVS Polar Pathfinder data set and AVHRR Polar Pathfinder data set as well as in surface observations. Schweiger (2004) attributes the increase in spring cloudiness to an increase in cyclonic activity with lower surface pressures. However, Kay et al. (2008) reasoned that the 2007 record-breaking minimum sea ice extent minimum was due to decreased summer cloudiness and increased shortwave radiation reaching the surface. Kay et al. (2008) conclude that, when the sea ice is thin, it's extent is increasingly subject to year-to-year variations in atmospheric circulation, cloudiness and intensity of shortwave radiation.

This paper examines the use of the satellites CloudSat and Calipso's data products, ECMWF-AUX and GEOPROF-lidar, in the Western Canadian High Arctic. Field data was collected over sea ice and the open ocean in the Beaufort Sea and Amundsen Gulf during the Circumpolar Flaw Lead System Study (CFL), 2008 (Barber et al., 2010) and the Arctic-Net Cruise, 2009. A Radiometrics microwave profiler (MWRP) and a Vaisala ceilometer ran continuously throughout both field campaigns giving detailed information about temperature and humidity profiles, plus cloud base height and cloud coverage.

The objective of this paper is to determine the reliability of ECMWF-AUX and GEOPROF-lidar data products in a high latitude polar environment by using statistical comparisons between satellite products and ground-based instrumentation. The analysis was performed in two parts: [1] Simultaneous MWRP measurements were compared to ECMWF-AUX temperature and absolute humidity profiles from the surface to 10 km and; [2] Cloud base heights from ceilometer and the MWRP measurements were compared to CloudSat and Calipso's combined GeoProf-lidar product.

3.2 Field Data

Field data was collected over two years, 2008 and 2009. During 2008 the University of Manitoba led an International Polar Year (IPY) project called The Circumpolar Flaw Lead System Study (CFL). The CFL project was an overwintering campaign in the Amundsen Gulf (70.5 °N; 124.0 °W) supported by the Canadian Coast Guard Ship (CCGS) Amundsen - Canada's research icebreaker (Barber et al. 2010). The CFL project collected data from November 2007 to August 2008. The ArcticNet cruise, from July until November 2009, an intensive field study centered in the Southern Beaufort Sea, was also supported by the CCGS Amundsen. The atmospheric sampling programs during CFL and ArcticNet provided a unique opportunity to monitor cloud cover and cloud properties, upper level and boundary layer temperature, and humidity in a polar environment. The two instruments, which were deployed during both CFL and ArcticNet, were the Radiometrics TP/WVP 3000 microwave profiling radiometer (MWRP) and the Vaisala CT25K Ceilometer.

3.2.1 Microwave Profiling Radiometer

The microwave profiler provided high temporal resolution ($\approx$ 1 minute) atmospheric profiles of temperature (K), and absolute humidity (10^{-3} kg m^{-3}) up to 10 km. The MWRP uses passive microwave radiometry at 22 – 29 GHz, and 51 – 59 GHz. The instrument also contains a sensor for surface pressure, and a zenith-pointing infrared radiometer (9.6–11.5 μm), to provide cloud-base temperature (TIR). The cloud base height is estimated from the intercept between TIR and the temperature profile. There can be ambiguity when there is a temperature inversion present, however this is accounted for using the relative humidity profile (Ware et al., 2003).

The MWRP provided volumetric measurements of temperature and humidity values at 50 meter intervals for 0 to 0.5 km, 100 meter intervals for 0.5 to 2 km, and 250 meters for 2 to 10 km. The profiles were processed in real-time giving nearly continuous monitoring of most of the troposphere interrupted only during moderate to heavy precipitation due to moisture on the radome. The temperature and humidity profiles were derived from microwave brightness temperatures using the manufacturer's neural network retrieval and radiative transfer model. The neural network was trained on historical radiosonde data from the upper-air station in Inuvik, Canada (68.30 °N; 133.47 °W). Figure 12 shows the MWRP mounted onboard the CCGS Amundsen.

From a comparison of the MWRP to radiosonde measurements, Candlish et al. (2011) concluded that the MWRP provided reliable measurements of both temperature and absolute humidity while mounted on the CCGS Amundsen. The RMS differences for temperature (RAOBS - MWRP) averaged 1.79 K through the lowest 2 km for January, February and March, 1.81 K for April, May and June, 2.51 K for July, August and September, and 2.47 K for October, November and December. Average biases of +0.99 K, +1.19 K, +2.13 K, and +2.08 K , respectively, indicated that the MWRP measurements were colder than the

Figure 12: The MWRP mounted onboard the CCGS Amundsen.

RAOBS for the lowest 2 km. For all seasons the RMS differences and biases for temperature increased with height above 2 km. Again the biases were all positive indicating the MWRP consistently recorded lower temperatures than the RAOBS. Candlish et al. (2011) also concluded that the MWRP measurements for humidity were slightly drier than the RAOBS for the lower 2 km. The RMS differences for humidity decreased greatly with height, with each season approaching 0.0 kg m^{-3} at heights greater than 6 km.

Candlish et al. (2011) also calculated the vertical resolution using the inter-level covariance method as defined by Smith et al. (1999). They found that the vertical resolutions were in general as coarse as the height measured, but concluded that this could be a result of the methodology. They concluded, from the statistical comparison with radiosondes and from a case study, that the MWRP had higher vertical resolution than that indicated by the inter-level covariance method.

3.2.2 Ceilometer

The Vaisala CT25K Ceilometer is a surface based instrument that uses LIDAR technology to detect the cloud base height for up to 7.6 km and for up to 3 layers of clouds. Besides cloud layers it can detect if there is precipitation or another obstruction to the viewing field. During CFL and ArcticNet 2009, the ceilometer was mounted behind the bridge on the port side of the Amundsen, at a 90 degree angle to ensure a clear view of the sky, Figure 13.

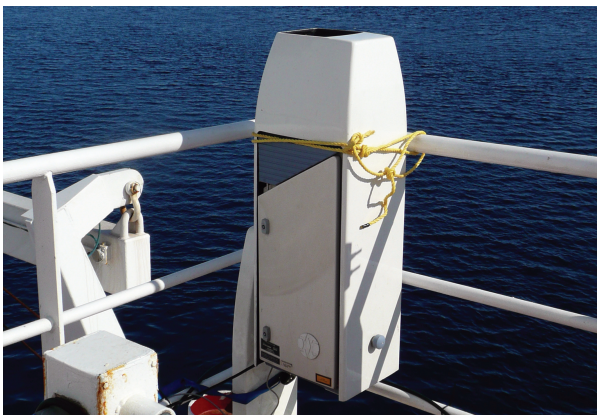

Figure 13: The ceilometer mounted onboard the CCGS Amundsen.

The ceilometer digitally samples the return echo every 100 ns from 0 to 50 μs, giving a vertical resolution of 15 m from the ground to approximately 7.6 km (Vaisala, 2002). Water droplets and ice crystal particles at all heights will cause a backscatter from the laser pulse. Since the fog and precipitation will attenuate the pulse, the cloud base height will appear lower in magnitude in the return echo.

3.3 CloudSat and Calipso

Satellite remote sensing is a vital source of information which can give global coverage for atmospheric variables and cloud properties. The difficulty and expense of mounting field programs is the main reason that satellite data is widely used for detection and measurement of cloud parameters in the Arctic. The satellites CloudSat and Calipso were designed by NASA's Jet Propulsion Laboratory and Colorado State University and launched in 2006 into sun-synchronous orbit. Calipso followed CloudSat to provide near simultaneous measurements. CloudSat's 94 Ghz cloud profiling radar (CPR) and Calipso's (Cloud-Aerosol Lidar and Infrared Pathfinder Satellite Observation) 532 nm and 1064 nm Cloud-Aerosol Lidar with Orthogonal Polarization (CALIOP) lidar are the first satellites with the capability to vertically profile the structure of Arctic clouds (Stephens et al., 2002). The combined radar-lidar cloud detection technique relies on the backscattered energy from cloud particles. The weak thermal and albedo contrasts between clouds and the ice-covered Arctic surface make other cloud detection techniques, which rely on passive radiances, deficient in the Arctic.

The ECMWF-aux product is generated from data produced by the European Center for Medium Range Weather Forecasting (ECMWF) global data set. The ECMWF data is interpolated into the CloudSat vertical bins. The ECMWF-aux gives the temperature, pressure and specific humidity profiles. These data along with the initial CPR data are required for input into the algorithms that produce the level 2 data products (CIRA, 2007).

2B-GeoProf-lidar is a combined data product from CloudSat's CPR and Calipso's CALIOP (lidar). The CPR has the ability to detect optically thick layers and with the lidar's ability to sense optically thin layers and tenuous cloud tops a combined data product has the potential to profile the complete atmosphere. The GeoProf-lidar data product aims to provide the best description of the occurrence of hydrometeor layers as well as the fractional volume of

clouds (Mace, 2007).

CloudSat and Calipso have different vertical and horizontal resolutions, with CloudSat's CPR having a footprint of 1.4 km by 2.5 km and a vertical resolution of approximately 0.25 km and Calipso's lidar having a footprint of 0.3 km by 0.3 km to 1 km and a variable vertical resolution of 0.03 km to 8.2 km. The GeoProf-lidar algorithm uses the spatial grid determined by the CPR (Mace, 2007).

3.4 Climatological Conditions during CFL and ArcticNet

There were 72 data sampling sites, where CloudSat and Calipso passed within 50 km of the ship's location in 2008 and 2009, Figure 14. The profiles for these locations were grouped by season. Arctic winter defined as January, February, and March (JFM) 2008; spring as April, May, and June (AMJ). All the data collected in spring was from 2008. Summer was July, August, and September (JAS). The summer data was collected during both the 2008 and 2009 field campaigns. Fall was defined as October, November and December (OND). The fall data were collected during the ArcticNet cruise in 2009, which included the returning trip to Quebec City through the North-West Passage. No data were collected during December 2009 as the ship left the Arctic Circle in mid November. There were a total of 23 comparable profiles during JFM, 23 during AMJ, 17 during JAS and 9 during OND.

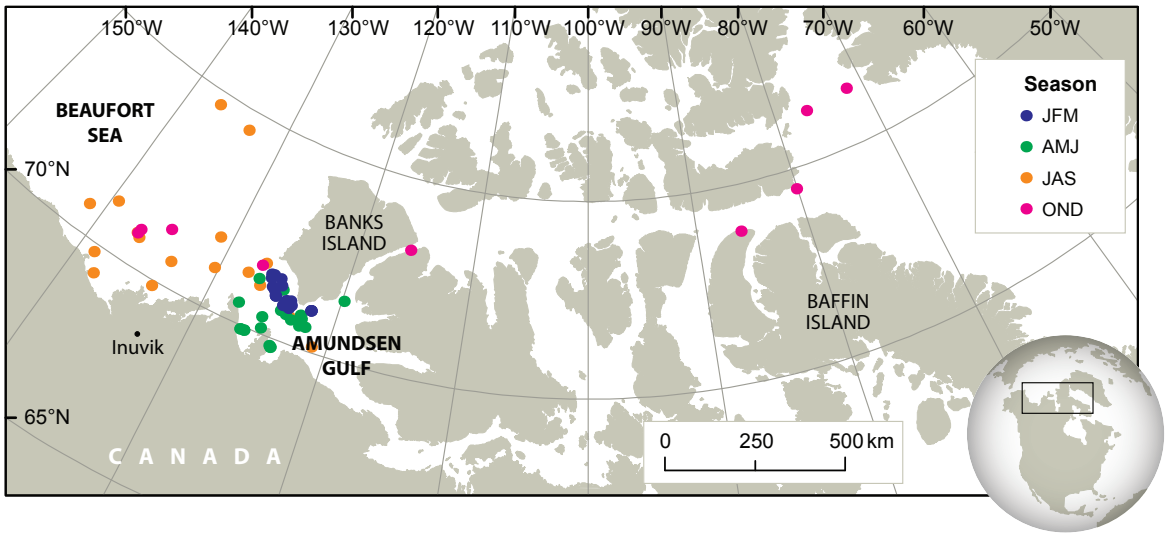

Figure 14: A map of the study region. The location of each of the 72 ECMWF-aux data points are shown, the colour represents the season: JFM - blue, AMJ - green, JAS - orange, OND - pink.

To assess the breadth of the climate conditions in our sample, mean temperature and absolute humidity profiles were calculated from the MWRP data. Figure 15, shows the mean temperature and range, left, and the mean absolute humidity and range, right, for each of the seasons. The mean winter profile had a temperature inversion in the lowest 1 km with a lapse rate of approximately 2.1 K/km, Figure 15a. The average surface air temperature during JFM was 249.5 K. All temperatures were below freezing with a maximum surface temperature of 261 K. The dryness of the Arctic winter is indicated by the absolute humidity profile, Figure 15a. The mean absolute humidity for the lowest 1 km was 0.58 x 10^{-3} kg m^{-3}. During JFM, the CCGS Amundsen operated in drift mode; the ship parked in a large, thick, homogeneous ice pan (first year ice >90 cm thick) until the ice condition or movement required the ship to move (Barber et al., 2010). The surrounding ice concentrations were $9+/10^{ths}$ with regions of mixed ice and open leads. High concentrations of thick sea ice act as a barrier between the atmosphere and the ocean reducing the transfer of heat and moisture (Barry et al., 1993). Figure 15b shows the mean temperature and absolute humidity profiles for AMJ. The mean surface temperature was still below freezing (267.6 K). The maximum surface temperature in the sample was 278.1 K. During the spring season the ice began to break up and melt ponds developed. With the decrease in ice, there was more moisture in the atmosphere than in winter. This is indicated by the mean absolute humidity profile. The absolute humidity at the surface had a mean of 3.0 x 10^{-3} kg m^{-3} and a range from 0.9 to 5.7 x 10^{-3} kg m^{-3}. Figure 15c shows the mean temperature and absolute humidity profiles for the summer months. During JAS the surface temperatures were generally above the freezing point. Mainly open water surrounding the ship. The Amundsen occasionally went further north into multiyear ice but generally stayed in the Southern Beaufort Sea. The surface temperature had a range of 271.6 to 289.9 K, and a mean of 277.0 K. With warmer temperatures and mainly open water, summer had the most moisture in the atmosphere as is indicated by the absolute humidity profiles. Figure 15d shows the atmospheric temperature and absolute humidity profiles for the fall. During October and November, freeze-up occurred. The mean surface temperature dropped below the freezing level to 266.2 K, and new first year ice began to develop. The surface tempera-

tures ranged from 262.2 to 272.1 K during this period. As the sea ice formed and thickened it started to form a barrier between the ocean and the atmosphere reducing the exchange of sensible and latent heat. The moisture in the atmosphere decreased due to the falling temperatures and increased ice cover to a mean surface value of 2.34 x 10^{-3} kg m^{-3}. The range was 1.68 to 4.05 x 10^{-3} kg m^{-3}.

The standard deviations of the MWR profiles were calculated for each of the CloudSat bin heights. Figure 16 shows the standard deviation for temperature, left, and the standard deviation for absolute humidity, right, for each of the seasons. The standard deviation for temperature was the smallest in JFM with the values remaining below 5 K and generally decreasing with height. JFM also had the smallest standard deviation for absolute humidity with a maximum value of 0.42 x 10^{-3} kg m^{-3} at a height of 1.4 km. The standard deviation of temperature in JAS remains below 6 K with a maximum of 5.8 K just above the surface at a height of 0.5 to 0.7 km. For JAS the maximum standard deviation of absolute humidity was 1.6 x 10^{-3} kg m^{-3}. The maximum standard deviation for absolute humidity was at the surface and decreased with height. The standard deviations at the surface were the greatest in the spring for both temperature and humidity, with values of 7.0 degrees and 3.0 x 10^{-3} kg m^{-3} respectively. The standard deviation for temperature had a maximum value of 9.2 degrees just above the surface at 0.2 km for AMJ. In OND the standard deviation of temperature was 4.1 degrees at the surface and increased in height to a maximum value of 8.1 degrees at a height of 5.8 km. The standard deviation then decreased with height. The standard deviation of absolute humidity, in OND, had a maximum value of 0.86 x 10^{-3} kg m^{-3} and decreased with height.

During CFL the atmospheric data was collected from January to August 2008. This data combined with the ArcticNet summer cruise data from July to November 2009 was collected during each of the four seasons and over a variety of ocean surfaces from $0/10^{ths}$ sea ice concentration to $10/10^{ths}$. The minimum surface temperature recorded in the sample was

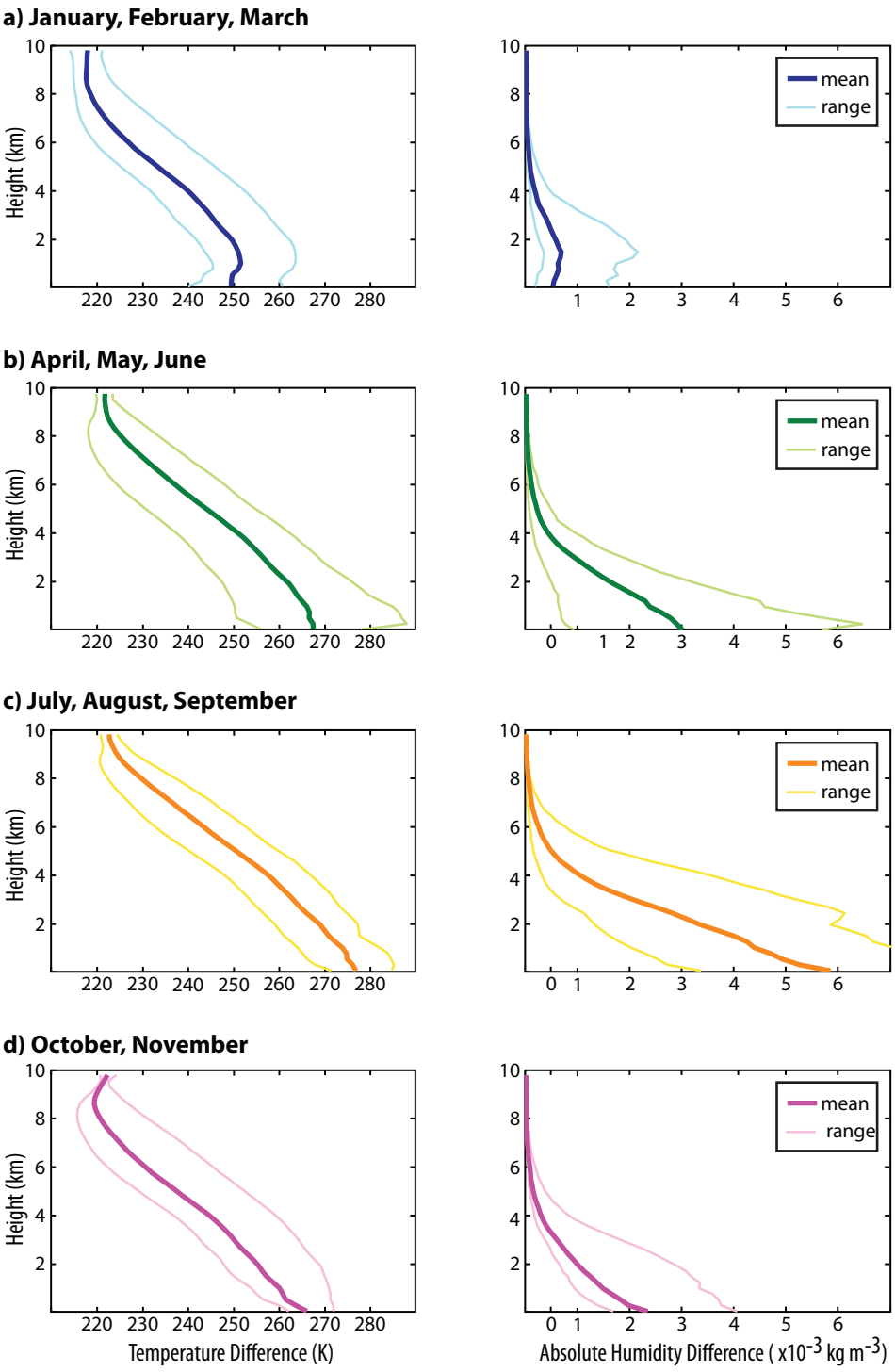

Figure 15: The mean atmospheric profile measured by the MWRP for temperature, left, and absolute humidity, right. The data were categorized by seasons (JFM, AMJ, JAS and OND).

-33°C with a maximum surface temperature of 12°C. During the sample period the weather observations recorded conditions that varied from clear skies to $8/8^{ths}$ cloud coverage to fog. Precipitation ranged from light snow flurries to moderate snow events and light to moderate rain. With such a varied environment during the seasons, the ECMWF-aux, GeoProf-lidar and MWRP data sets covered a broad range of weather and surface conditions.

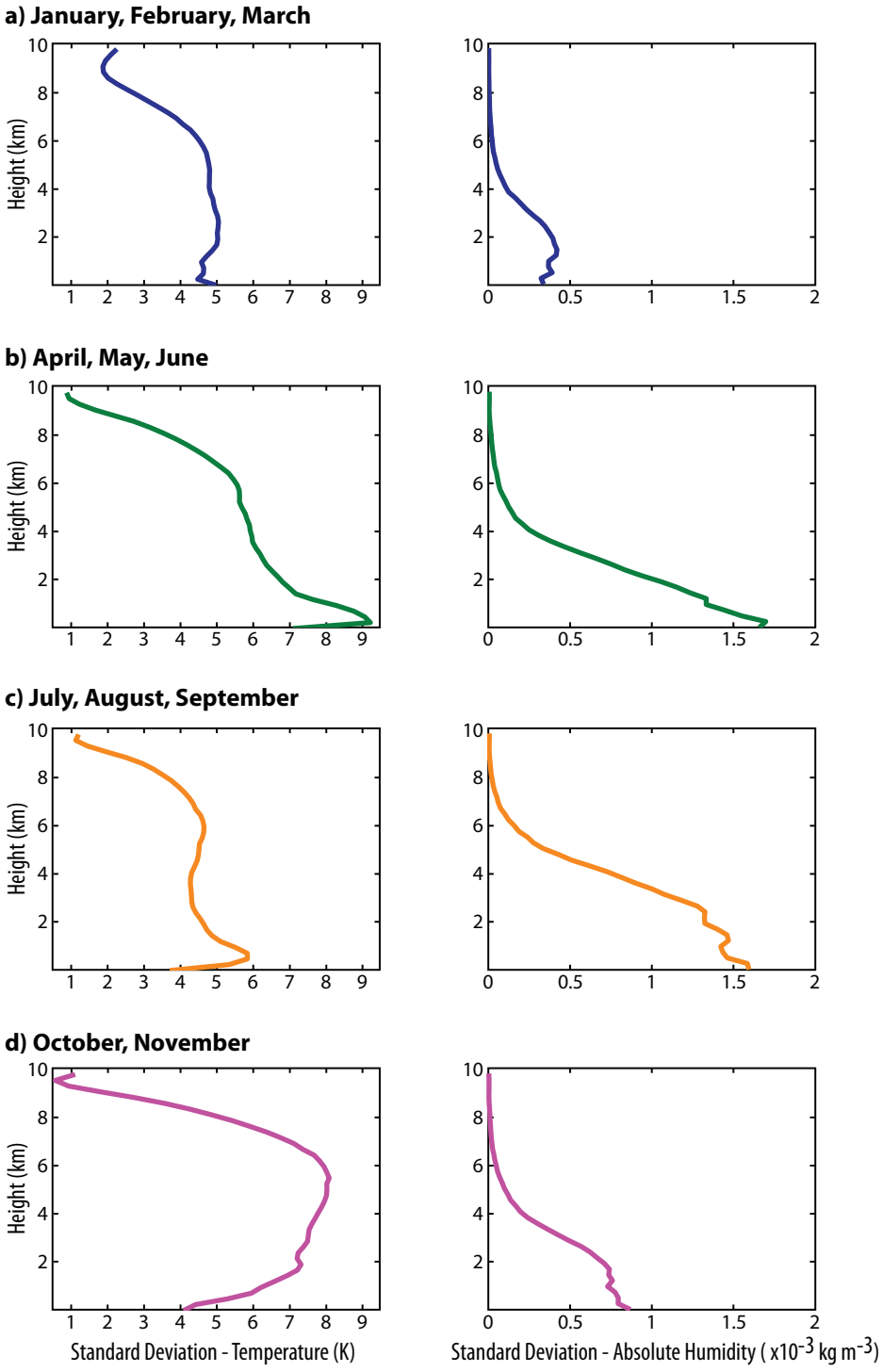

Figure 16: The standard deviation of the atmospheric profiles measured by the MWRP for temperature, left, and absolute humidity, right.

3.5 Validation of ECMWF-aux

The first objective of this study was to determine how the CloudSat's ECMWF-aux atmospheric temperature and absolute humidity profiles compared to profiles from a ground-based instrument. Absolute humidity profiles were calculated from the specific humidity, pressure and temperature in the ECMWF-aux data product. The temperature and absolute humidity measurements from the MWRP was linearly interpolated to CloudSat's bin heights.

The root-mean-square difference and bias between the MWRp and the ECMWF-aux data were calculated for each of the CloudSat bin heights. The bias were calculated as the MWRP minus the ECMWF. Figure 17 shows the RMS difference and bias profiles for temperature, left, and absolute humidity, right, for each of the four seasons. The average RMS difference for the lower 1 km of the atmosphere during JFM was 8.4 K, with the RMS increasing with height to a maximum of 29 K at approximately 10 km. The RMS differences for absolute humidity during JFM had a surface value of 0.8 x 10^{-3} kg m^{-3} with a maximum value of 1.3 x 10^{-3} kg m^{-3} at 1.9 km. During AMJ, for temperature, the average RMS difference below 1 km was 9.8 K, where the average RMS difference from 1 to 5 km was 11.3 K, increasing to a maximum RMS difference of 17 K at 9.1 km. The RMS difference for absolute humidity at the surface was 1.6 x 10^{-3} kg m^{-3} with a maximum value of 2.9 x 10^{-3} kg m^{-3} at 1.7 km. During JAS the RMS difference for temperature at the surface was 12.7 K. The RMS then dropped to 5.3 K at approximately 0.2 km. The maximum RMS difference was at 6.7 km with a value of 19.4 K. The absolute humidity during JAS, had a maximum RMS difference of 4.0 x 10^{-3} kg m^{-3} at the surface and it decreased with height. During fall, the RMS difference for temperature remained relatively constant with a range from 7.5 to 10.2 K. The RMS difference for absolute humidity had a surface value of 1.21 x 10^{-3} kg m^{-3} and a maximum of 1.4 x 10^{-3} kg m^{-3} at a height of 0.7 km. Although the average bias for temperature at each height was relatively small for each season the RMS

difference was relatively large. This indicated that the CloudSat ECMWF-aux temperature profiles should be viewed with scepticism as there were large random errors. During spring and summer the RMS differences for absolute humidity were the greatest. This was to be expected, as the moisture in the air was the greatest during these two seasons. All of the seasonal biases again were relatively small compared to the RMS differences. Overall, it was concluded that the absolute humidity from the surface to approximately 2 km should be viewed as suspect during the spring and summer seasons.

Figure 18 shows the frequency distribution of the bias with height. The bias was calculated as the MWRP minus the ECMWF for the 72 sampling points covering all seasons. The temperature biases were divided into class intervals with a width of 1 K. The absolute humidity biases were divided into class intervals with a width of 0.5 x 10^{-3} kg m^{-3}. Looking at the distribution of the temperature bias, left, the graphs show nearly normal distributions for all heights except 9.8 km. However, the distributions are not centered on zero. This indicates that the errors are, in all likelihood, systematic. The surface biases have a positive shift. The other levels from 0.5 km to 5 km also have a normal distribution, however unlike the surface they show a negative offset. This shows that the ECMWF-aux indicated higher temperatures than the MWRP from approximately 0.5 km to 5 km. That is, the ECMWF-aux temperatures for height levels from 0.5 km to 5 km have a warm bias. As height increased the bias increased. At 9.8 km, the distribution is centered on zero, however the distribution curve is multimodal rather than normal. For the absolute humidity, on the right, the bias decreased with height. The surface distribution was positively shifted. This may indicate a systematic error. At higher altitudes, the moisture in the air was less, thus the bias distribution became smaller.

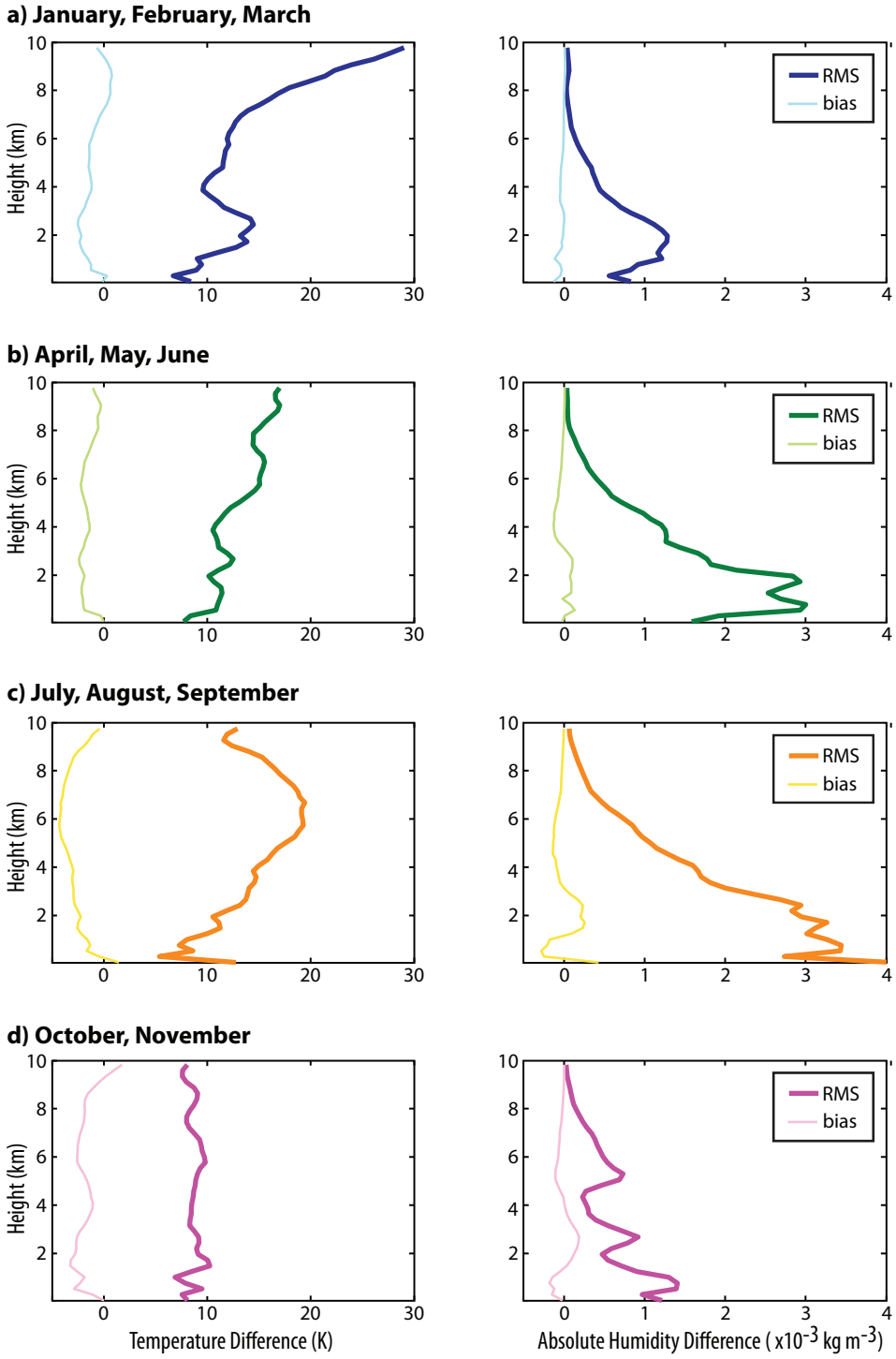

Figure 17: The root-mean-square difference, and bias versus height in kilometers for temperature on the left and absolute humidity on the right, from Radiometrics microwave profiling radiometer and CloudSat's ECMWF-aux data. The bias was determined by the MWRP minus the ECMWF-aux data.

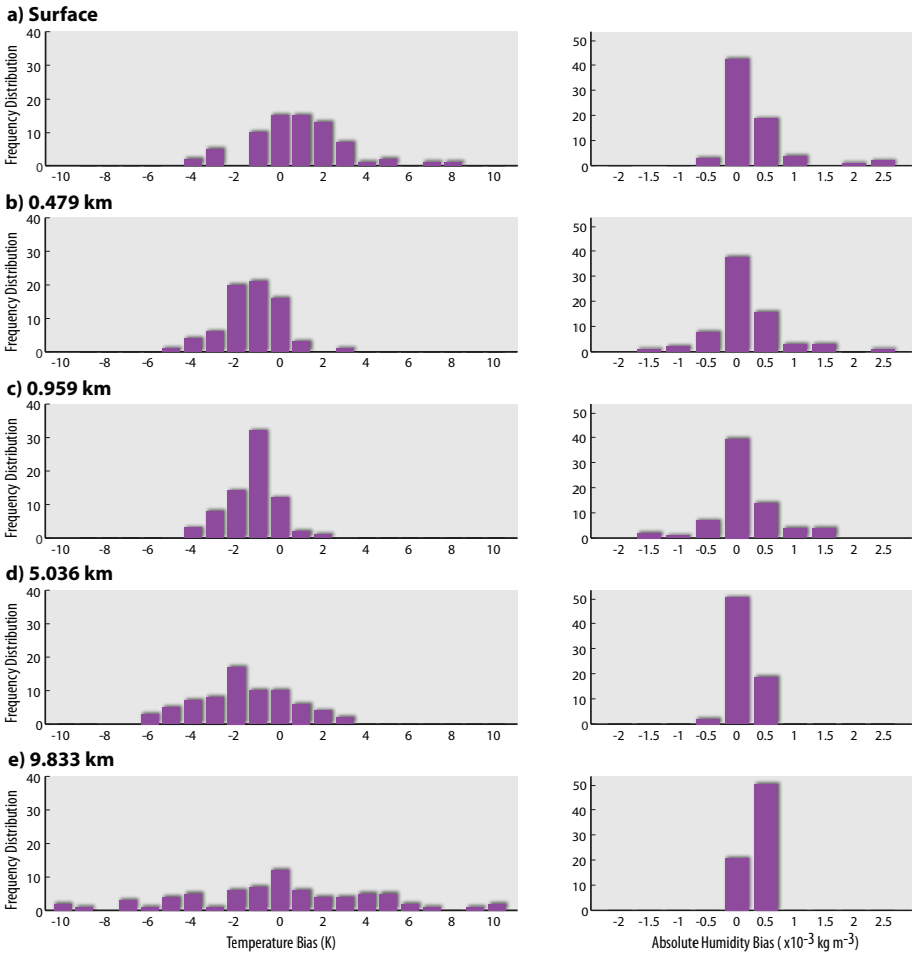

Figure 18: The frequency distribution of the ECMWF-aux bias. The data were grouped by heights, a) 0 km, b) 0.479 km, c) 0.959 km, d) 5.036 km and e) 9.833 km. The bias was the MWRP minus the ECMWF-aux data.

3.6 Validation of GeoProf-lidar

Cloud base height measured by the ship mounted laser ceilometer and MWRP were compared to the GeoProf-lidar output to assess the latter's accuracy. This was accomplished by comparing 67 sample times where the satellites passed within 50 km of the Amundsen's location, Figure 19. There were a total of 20 comparable measurements during JFM, 21 during AMJ, 17 during JAS and 9 during OND.

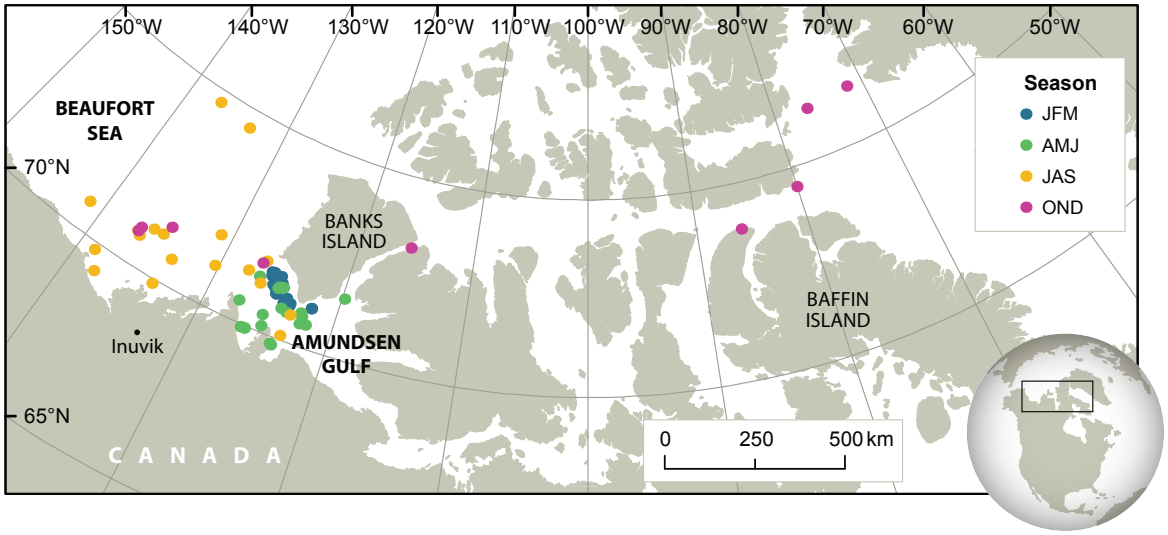

Figure 19: A map of the study region. Locations of the each of the 67 CloudSat and Calipso GeoProf-lidar data points are shown. The colour represents the season: JFM - blue, AMJ - green, JAS - orange, OND - pink.

Figure 20 shows the median hourly values of the cloud base height for January 1st to August 5th 2008. Similarly, Figure 21 shows the median hourly values from July 16th to November 4th 2009. These two figures show an overview of the cloud coverage during both field seasons. The MWRP operated continuously throughout both field seasons with the exception of times when the profiler was being calibrated. Similarly the ceilometer provided continuous cloud base height throughout both field seasons unless the instrument's viewing

field was blocked by frost, precipitation or debris. The MWRP and the ceilometer use different techniques to measure the cloud base heights and as such they often disagreed on the heights, with the ceilometer generally measuring low clouds more often than the MWRP. The ceilometer is the standard when measuring cloud base height, however during the 2008 and 2009 field seasons the ceilometer measured only a single layer of clouds; multiple layers were never recorded. The MWRP cloud base height was used in the comparison with the GeoProf-lidar data to verify that if multiple layers of clouds existed, the higher clouds were recorded. The occurrence of fog measured by the MWRP and not by the ceilometer is due to the ceilometer's technical limitation that it only measures clouds with a base height above 50 meters.

Table 2 shows the total operational hours, total hours missing data and the total hours for low, middle and high clouds during each season for 2008 and 2009. By our definition, low clouds had base heights 2 km and below, middle were between 2 to 4 km and high clouds had base heights greater than 4 km. During JFM 2008 there was a total of 2184 operational hours with 85.2% being cloud free as measured by the MWRP and 69.8 % cloud free as measured by the ceilometer. The MWRP was missing data for a total of 43 hours or 2.0 % while the ceilometer was missing data for a total of 110 hours or 5.0 %. The MWRP and ceilometer differed in their cloud measurements. The ceilometer measured a considerably higher number of hours with low clouds, 19.3 % of the time versus 8.0 % by the MWRP. The MWRP also measured 11 hours of fog (0.5% of the time).

During AMJ, there was a total of 2184 total operation hours. The MWRP measured 60.2% of the time to be cloud free, while the ceilometer measured 44.9%. Over the three months AMJ, the ceilometer measured 36.7% of the time to be low cloud while MWRP measured 27.5%. The MWRP also measured 34 occurrences of fog (1.5% of the time). During July and August 2008 the ceilometer and MWRP had a total of 840 total operational hours with the MWRP missing data for 34 hours or 4.0% and the ceilometer missing data for 31 hours

or 3.7%. The MWRP and ceilometer measured cloud free hours for half of the time with 48.9% measured by the MWRP and 52.3% measured by the ceilometer. During 2008 the field season ended in August, with no data recorded during September or during the fall months.

Table 1: The hourly median cloud base height as measured by the MWRP and ceilometer. Each value is the hours per season.

	JFM 2008	AMJ 2008	JAS 2008	JAS 2009	OND 2009
Operational Hours	2184	2184	840	1800	816
MWRP Data					
Missing Data	43 (2.0%)	1 (0.0%)	34 (4.0%)	44 (2.4%)	7 (0.9%)
Cloud Free	1861 (85.2%)	1315 (60.2%)	411 (48.9%)	477 (26.5%)	289 (35.4%)
Low Clouds	174 (8.0%)	600 (27.5%)	268 (31.9%)	969 (53.8%)	427 (52.3%)
Mid Clouds	88 (4.0%)	220 (10.1%)	93 (11.1%)	251 (13.9%)	70 (8.6%)
High Clouds	18 (0.8%)	48 (2.2%)	34 (4.0%)	59 (3.3%)	23 (2.8%)
Ceilometer Data					
Missing Data	110 (5.0%)	353 (16.2%)	31 (3.7%)	705 (39.2%)	1 (0.1%)
Cloud Free	1525 (69.8%)	980 (44.9%)	439 (52.3%)	255 (14.2%)	129 (15.8%)
Low Clouds	421 (19.3%)	801 (36.7%)	283 (33.7%)	840 (46.7%)	684 (83.8%)
Mid Clouds	118 (5.4%)	50 (2.3%)	80 (9.5%)	0 (0.0%)	2 (0.2%)
High Clouds	10 (0.5%)	0 (0.0%)	7 (0.8%)	0 (0.0%)	0 (0.0%)

In 2009 there was a total of 25 GeoProf lidar measurements. During JAS 2009 there was a total 1800 operational hours, 26.5% with the median value being cloud free as measured by the MWRP and 14.2% cloud free measured by the ceilometer. The MWRP was missing data for a total of 44 hours or 2.4% while the ceilometer was missing data for a total of 705 hours or 39.2%. The ceilometer only recorded low clouds (base heights below 2 km) while the MWRP had middle clouds 13.9% of the time and high clouds 3.3% of the

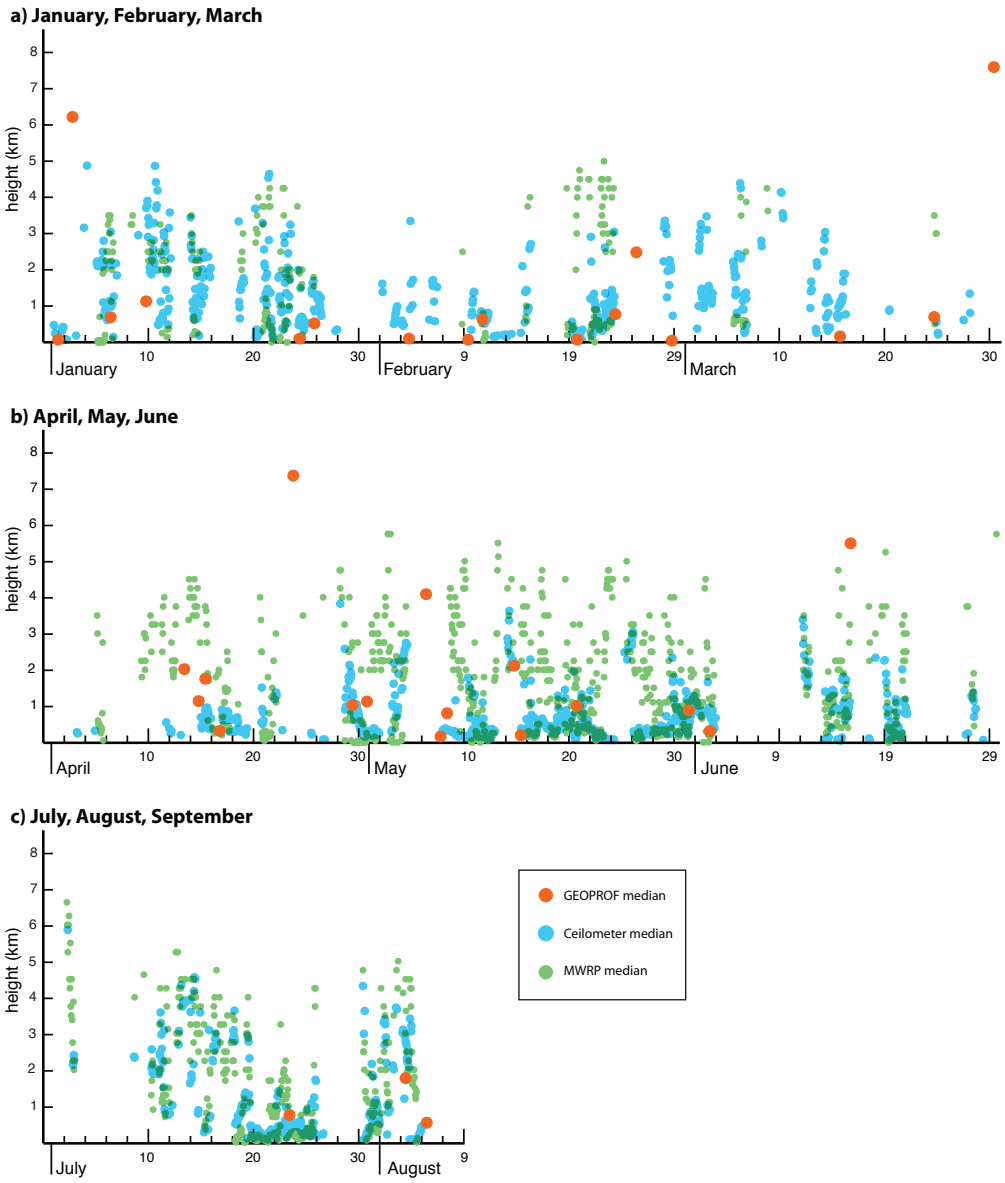

Figure 20: The median hourly cloud base height for 2008. The cloud base height measured by the ceilometer is shown in blue, the MWRP is shown in green and the GeoProf-lidar is shown in orange.

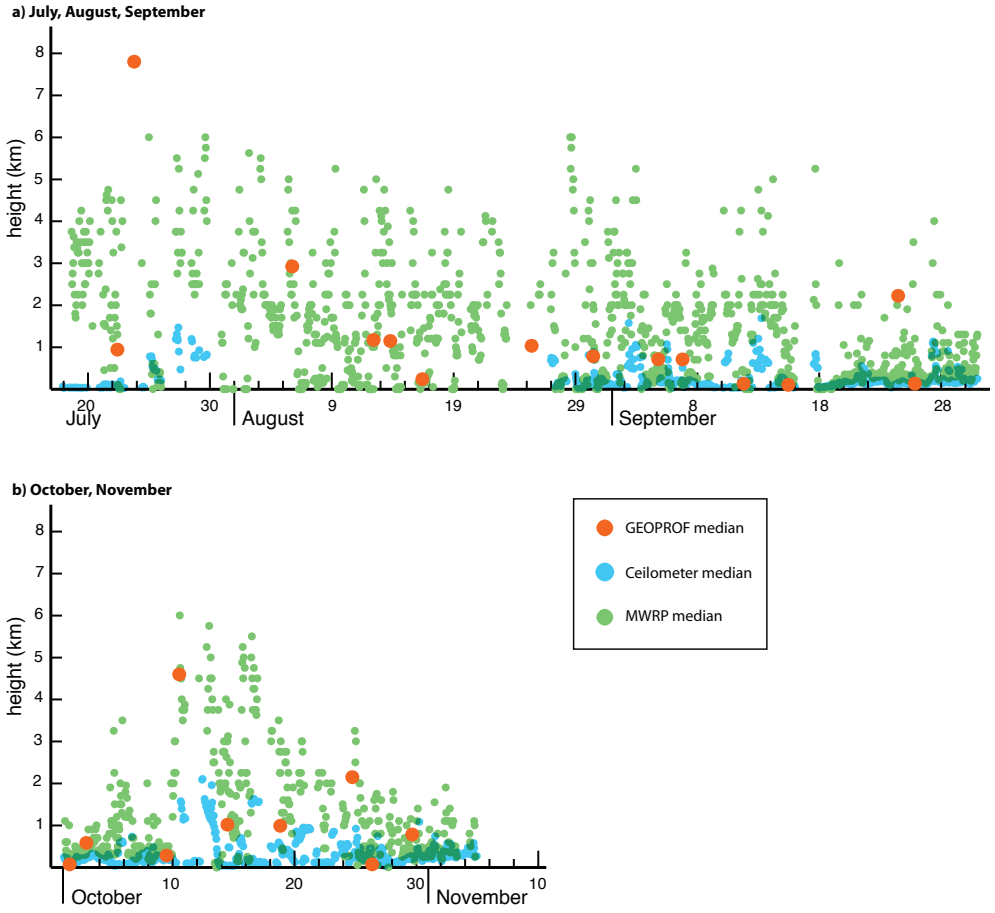

Figure 21: The median hourly cloud base height for 2009. The cloud base height measured by the ceilometer is shown in blue, the MWRP is shown in green and the GeoProf-lidar is shown in orange.

time. The MWRP also measured 97 occurrences of fog(5.4% of the time). During October and November 2009 the MWRP and ceilometer were only operational for 816 hours. The MWRP measured 35.4% of the time cloud free while the ceilometer measured 15.8%. The MWRP was missing data for 7 hours (0.9% of the time) while the ceilometer was missing data for only 1 hour (0.1% of the time). The Ceilometer again measured most hours with low clouds, 83.8% of the time, while the MWRP measured only 52.3%.

Figure 23 shows the median cloud base height and range for every occurrence of the CloudSat and Calipso's GeoProf-lidar data product in our sample. The GeoProf-lidar median cloud base height was calculated from only the clouds viewed while the satellites' ground track was within a 50 km range of the CCGS Amundsen. The MWRP and the ceilometer medians were calculated using a two-hour window surrounding the satellites pass. The two-hour window was used to compensate for the satellite passing up to 50 km from the ship. The two-hour interval was considered adequate time for the air parcel measured by CloudSat and Calipso to pass over the ship and be observed by the MWRP and ceilometer. Figure 22 shows an example of the geo-spatial comparisons between the GeoProf-lidar data and the ceilometer and MWRP while mounted on the CCGS Amundsen. In order to compare only the cloud base heights, clear sky measurements were removed from the time series for calculations of the median and range. There is considerable disagreement between the cloud base heights measured by the instruments, Figure 23. The ceilometer mainly measured low clouds while the MWRP consistently measured a higher occurrence of middle and high clouds. There were several occurrences when the GeoProf-lidar indicates clouds when both the ceilometer and microwave profiler measured clear skies.

Figure 24 shows the frequency distribution of the biases for the cloud base medians. The biases were calculated as the ceilometer heights minus the GeoProf-lidar heights, on the left in blue. There were a total of 58 comparable measurements for the ceilometer. On the right, in green, is the frequency distribution for the microwave profiler minus the GeoProf-

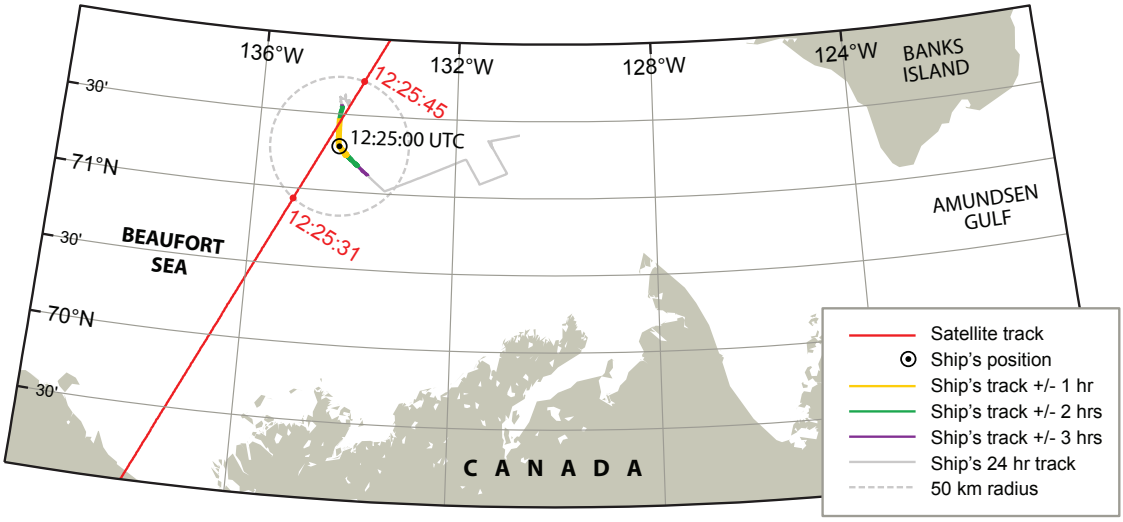

Figure 22: An example of how the spatio-temporal comparisons were made between CloudSat and Calipso's GeoProf-lidar data and the MWRP and ceilometer data while mounted on the CCGS Amundsen.

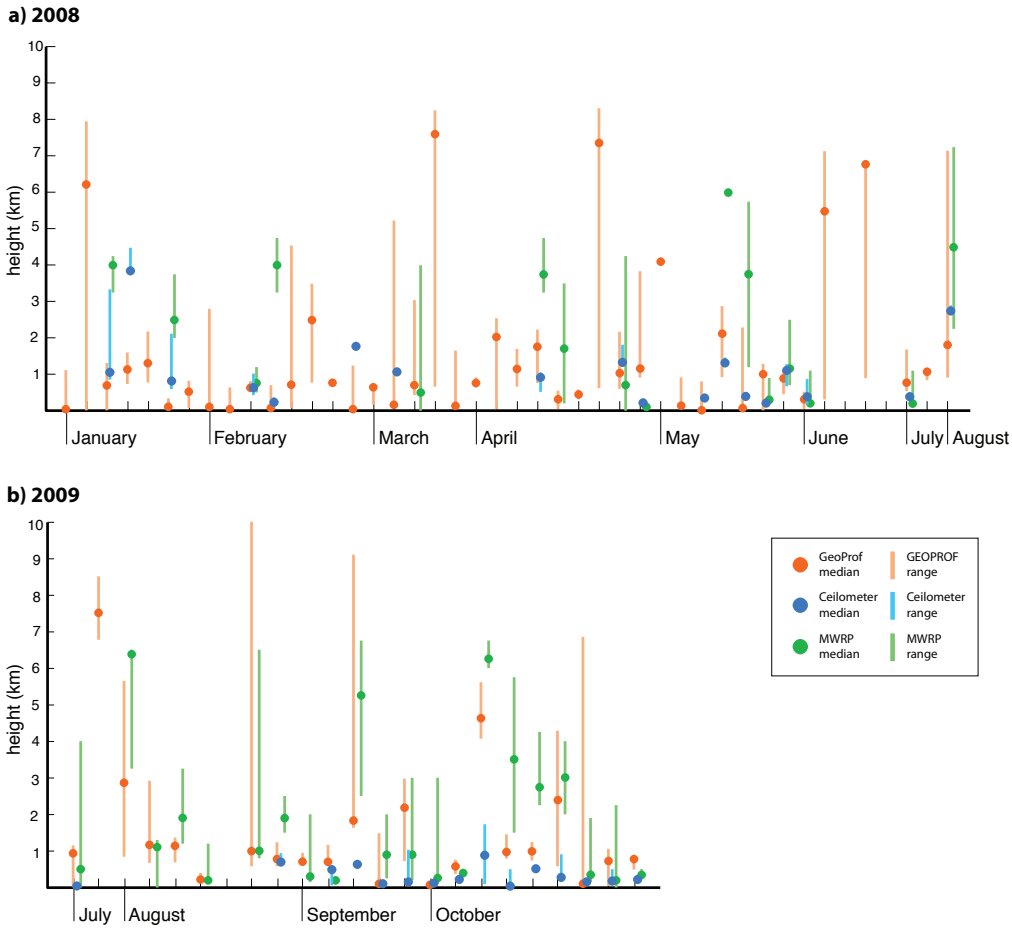

Figure 23: The median cloud base height and range. The ceilometer is shown in blue, the MWRP is shown in green and the GeoProf-lidar is shown in orange.

lidar biases. There were a total of 67 comparable measurements for the MWRP. For the ceilometer and microwave profiler, the median cloud base heights (with clear skies removed) were used for the two, four or six hours surrounding the satellite pass, Figure 24a, b and c. The biases were divided into class intervals with a width of 500 meters, centered on 0. On each subplot, Figure 24, the orange bar indicates the number of occurrences when the GeoProf-lidar measured clouds and either the ceilometer or the MWRP did not.

There were 15 "discrepancies" between the ceilometer, with a 6 hour window, and the GeoProf-lidar, Figure 24c. These discrepancies occurred when the ceilometer detected no clouds for 6 hours surrounding the satellite pass and the GeoProf-lidar reported clouds. This is only slightly lower than for the two-hour and for the four-hour interval shown in Figures 24a and 24b. The two-hour window had 19 and the four-hour interval that had 17 discrepancies. This is a large percentage of discrepancies considering there were only 58 total overlapping measurements. Similarly with the microwave profiler, there were a total of 25 times for the six-hour intervals when the GeoProf-lidar measured clouds and the MWRP did not. During the six-hour interval there were a total of 15 occurrences when neither the ceilometer nor the MWRP saw clouds but the GeoProf-lidar did. These "discrepancies" can be due to a number of causes. They could be due to callibration, or algorithm design flaws. The distance between the ship and the satellites ground track was likely a factor, although this was partially accounted for using up to six-hour time intervals or windows.

Table 2 shows the dates and times of the 15 occurrences when both the MWRP and the ceilometer measured clear skies but the GeoProf-lidar indicated clouds. The 15 "discrepancies" are spread out through three seasons. There were 8 during JFM, 5 during AMJ, 2 during JAS, and none in OND. The GeoProf-lidar data product contains a flag indicating, for each granule in the satellites' ground track, which instrument viewed the cloud. That is CloudSat's radar, Calipso's lidar, both the radar and the lidar, or neither the radar nor the lidar. Table 2 includes the percentage of granules for which each of the instruments

viewed cloud. The cloud base heights, Table 2, measured by GeoProf-lidar show that 7 of the 15 discrepancies had cloud base heights of less than 2 km. Due to a relatively small sample spread over a large time period it's hard to determine why there are so many of these discrepancies. Future field seasons could provide further insight into these outstanding issues.

Table 2: The 15 occurrences when the GeoProf-lidar indicates clouds when neither the MWRP nor the ceilometer measure clouds for 6 hours surrounding the satellites pass.

Date yyyy m d hh:mm	Median Cloud Base Height (m)	% radar	% lidar	% radar & lidar	% no cloud detected
2008 1 2 20:20	6220	11.0	89.0	0.0	0.0
2008 1 15 11:44	1305	23.1	3.3	1.1	72.5
2008 2 9 11:38	40	2.4	88.0	0.0	9.6
2008 2 25 11:38	2485	51.7	47.2	1.1	0.0
2008 2 26 20:27	764	3.8	0.0	0.0	96.2
2008 3 12 11:38	641	5.5	4.4	0.0	90.1
2008 3 30 11:26	7600	5.1	94.9	0.0	0.0
2008 3 31 20:14	130	19.0	21.5	0.0	59.5
2008 4 22 11:33	444.5	3.3	3.3	0.0	93.3
2008 4 23 20:21	7360	10.9	89.1	0.0	0.0
2008 5 6 11:45	4090	0.0	92.7	0.0	7.3
2008 6 15 20:39	5492.5	62.0	38.0	0.0	0.0
2008 6 18 11:27	6775	5.5	21.9	0.0	72.6
2008 7 26 20:34	1068	10.0	0.0	0.0	90.0
2009 7 23 21:14	7516	68.8	12.5	0.0	18.8

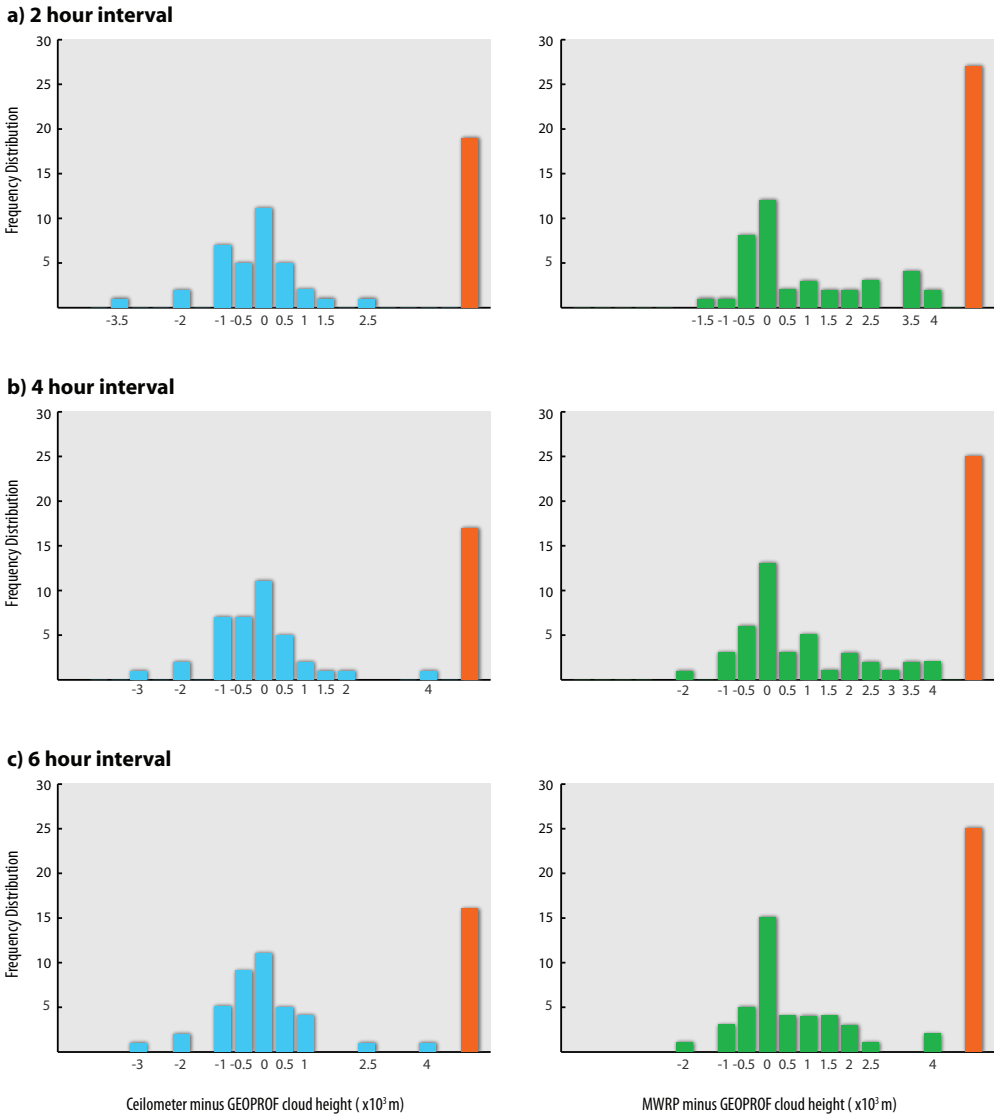

Figure 24: The frequency distribution of the GeoProf-lidar bias. The ceilometer and microwave profiler use the median cloud base height with clear skies removed for a) two, b) four or c) six hours surrounding the satellites pass. The bias was determined by the MWRP or ceilometer minus the GeoProf-lidar. The orange indicates occurrences when the GeoProf-lidar measured clouds and either the MWRP or the ceilometer had clear skies.

3.7 Discussion and Conclusions

In 2008-2009 a ship borne microwave profiler (MWRP) ran continuously, thus creating a time series for the Amundsen's location in the Arctic. When CloudSat's data product ECMWF-aux was compared with the microwave profiler, the temperature bias was negative, except near the ground indicating that the ECMWF-aux generally indicated warmer temperatures than the MWRP. The RMS differences for temperature showed a substantial disagreement between the temperature measurements from the two systems. The absolute humidity comparisons showed the best agreement in winter. This may be attributed to the Arctic's dry winter climate. The spring, summer and fall had much greater variations in the ocean surface, with sea ice concentrations ranged from $0/10^{ths}$ to $10/10^{ths}$. The variability of the ocean cover and ice thickness may have resulted in the larger humidity RMS differences between the two instruments during the spring, summer and fall. The resolution of the ECMWF-aux is based on the CloudSat bin heights; in order to compare the ECMWF-aux to the MWRP data the MWRP data was linearly interpreted to the CloudSat bin heights. The negative bias for temperature may be a factor of both the distance between the two measurements and the linear interpretation of the MWRP temperature and humidity data. Candlish et al. (2011) determined that the MWRP temperature and humidity data were less reliable with increasing height when compared to radiosonde measurements. This was likely a factor in the larger RMS differences, at heights greater than 4 km, between the MWRP and the ECMWF-aux temperature data.

As cloud base height can vary tremendously over a short distance, it is intrinsically difficult to compare two different measurements unless they are measuring the same air space. Measurements were only compared when the GeoProf-lidar was within 50 km of the CCGS Amundsen. The variability over this distance is likely a large factor in the cloud base height differences.

The in situ ceilometer and MWRP often indicated no cloud when CloudSat and Calipso did. The 15 discrepancies, when the GeoProf-lidar indicated cloud and neither ceilometer nor the MWRP recorded clouds for the 6 hours surrounding the time of the satellites' pass, leads us to be sceptical. The GeoProf-lidar algorithm aims for a false detection rate of 15% however our comparisons indicated that there is a false detection rate of 25%. The GeoProf-lidar flags indicated that 4 out of the 15 discrepancies had less than 10% of the granules measuring clouds. This suggests that the constraints used by the GeoProf-lidar data product for cloud detection may need to be refined to reduce the large number of apparently false detections.

Although the GeoProf-lidar data product has a large false detection rate in the Beaufort Sea, studies can still be done on the overall change and trends of cloud coverage over the Arctic. CloudSat and Calipso pass over twice a day and cover a large area of the Arctic; being launched in 2006 there is a large base of data that can be analysed to see what trends have been occurring over the Beaufort Sea and surrounding areas.

Acknowledgments

This work was partially funded by the Natural Sciences and Engineering Research Council (NSERC), the International Polar Year (IPY) Federal Program Office, and the Canada Research Chairs (CRC) programs through grants to D.G.Barber. Thanks to C.R. Candlish, J. Iacozza, S. Fargey and R. Scharien for their contributions. We would like to acknowledge the crew and captain of the CCGS Amundsen for their considerable help.

References

Barber, D. G., Asplin, M., Gratton, Y., Lukovich, J., Galley, R., Raddatz, R., and Leitch, D. (2010). The international polar year (ipy) circumpolar flaw lead (cfl) system study: introduction and physical system. *Atmos.- Ocean*.

Barry, R., Serreze, M., Maslanik, J., and Preller, R. (1993). The arctic sea ice-climate system: Observations and modeling. *Reviews of Geophys.*, 31(4):397.

Candlish, L. M., Raddatz, R., Asplin, M., and Barber, D. G. (2011). Veracity of atmospheric temperature and absolute humidity profiles over the beaufort sea and amundsen gulf from a microwave radiometer. *Journal of Atmospheric and Oceanic Technology - In Review*.

CIRA (2007). *CloudSat Project A NASA Earth System Science Pathfinder Mission: CloudSat Standard Data Products Handbook*. Cooperative Institute for Research in the Atmosphere, Colorado State University, Fort Collins, CO 80523.

Curry, J., Rossow, W., Randall, D., and Schramm, J. (1996). Overview of arctic cloud and radiation characteristics. *Journal of Climate*, 9(8):1731–1764.

Hahn, C., Warren, S., and London, J. (1995). The effect of moonlight on observation of cloud cover at night, and application to cloud climatology. *Journal of Climate*, 8(5):1429–1446.

Isaac, G. and Stuart, R. (1996). Relationships between cloud type and amount, precipitation, and surface temperature in the mackenzie river valley-beaufort sea area. *Journal of Climate*, 9:1921–1941.

Jin, X., Hanesiak, J., and Barber, D. (2007). Time series of daily averaged cloud fractions over landfast first-year sea ice from multiple data sources. *Journal of Applied Meteorology and Climatology*, 46(11):1818–1827.

Kay, J., L'Ecuyer, T., Gettelman, A., Stephens, G., and O'Dell, C. (2008). The contribution of cloud and radiation anomalies to the 2007 arctic sea ice extent minimum. *Geophysical Research Letters*, 35(8):L08503.

Mace, G. (2007). Level 2 geoprof product process description and interface control document algorithm version 5.3. *NASA Jet Propulsion Laboratory*.

Minnett, P. (1999). The influence of solar zenith angle and cloud type on cloud radiative forcing at the surface in the arctic. *Journal of Climate*, 12(1):147–158.

Schweiger, A. (2004). Changes in seasonal cloud cover over the arctic seas from satellite and surface observations. *Geophysical Research Letters*, 31(12):L12207.

Smith, W. L., Feltz, W. F., and and, R. O. K. (1999). The retrieval of planetary boundary layer structure using ground-based infrared spectral radiance measurements. *J. Atmos. and Oceanic Tech.*, 16:323–333.

Stephens, G., Vane, D., Boain, R., Mace, G., Sassen, K., Wang, Z., Illingworth, A., O'Connor, E., Rossow, W., Durden, S., et al. (2002). The cloudsat mission and the a-train. *Bulletin of the American Meteorological Society*, 83(12):1771–1790.

Tsay, S., Stamnes, K., and Jayaweera, K. (1989). Radiative energy budget in the cloudy and hazy arctic. *Journal of the Atmospheric Sciences*, 46(7):1002–1018.

Vaisala (2002). *Ceilometer CT25K User's Guide*. Vaisala, P.O. Box 26 FIN-00421 Helsinki, Finland, m210345en-a edition.

Walsh, J. and Chapman, W. (1998). Arctic cloud-radiation-temperature associations in observational data and atmospheric reanalyses. *Journal of Climate*, 11(11):3030–3045.

Ware, R., Carpender, R., Guldner, J., Liljegren, J., Nehrkorn, T., Solhelm, F., and Vandenberghe, F. (2003). A multichannel profiler of temperature, humidity, and cloud liquid. *Radio Science*, 38:1–44.

4 Conclusions and Recommendations

The overall theme of the thesis was to investigate remote sensing techniques for atmospheric temperature, humidity and cloud detection over the Arctic marine cryosphere. The data set collected is an extremely unique data set. The two field campaigns in 2008 and 2009 collected high temporal data for humidity, temperature, pressure and cloud base height, spanning every season. All data were collected in the Arctic marine environment for a variety of different surface types, from open ocean to thick consolidated sea ice. Other field campaigns in the Arctic have lacked the breadth spatially and temporally; generally concentrating on a single location close to shore and over a short summer field season. The data collected from 2008 and 2009 is an invaluable resource.

The main objective was to assess CloudSat and Calipso in the high Arctic. In order to compare the MWRP to the satellite data, the MWRP data needed to be validated. The first manuscript statistically compared radiosondes and MWR profiles for temperature and absolute humidity. Knowing that the MWRP gave reliable data led to the second manuscript, which compared the temperature and humidity profiles from the MWRP to CloudSat's ECMWF-aux data. This manuscript also compared the cloud base height data measured by the ceilometer and MWRP to CloudSat and Calipso's combined data product GeoProf-lidar. Using Radiometric's MWRP while mounted onboard a ship in the Arctic is a new approach to collecting data in a remote and under-studied area. The data were invaluable in validating the satellites CloudSat and Calipso in a marine polar environment.

The first objective of this thesis was to assess the veracity of a ship based microwave profiling radiometer in the Arctic. The study used a total of 68 radiosonde profiles to compare to corresponding radiometer profiles. The profiles were grouped by season and sea ice concentrations. With low concentrations of sea ice there was a larger bias for both temperature and absolute humidity. The larger bias with low concentrations of sea ice may be attributed

to the MWRP's neural network. The neural network was trained using historical radiosonde data from Inuvik, NWT, Canada, which is located inland approximately 100 km from the coastline. This may have introduced a bias close to the surface in the neural network coefficients, and may have led the MWRP to exhibit a dry bias, akin to the climate at Inuvik, rather than a marine climate.

The RMS difference and bias for each season were calculated as the RAOBS minus the MWRP. The RMS differences for temperature averaged 1.79 K through the lowest 2 km for winter, 1.81 K for the spring, 2.51 K for the summer, and 2.47 K for the fall. Average biases of +0.99 K, +1.19 K, +2.13 K, and +2.08 K, respectively, indicated that the MWRP measurements were colder than the RAOBS for the lower 2 km. Similarly, average biases for 2 to 10 km were all positive, indicating that the MWRP consistently recorded lower temperatures than the RAOBS. Our results compared reasonably well to other validation studies where Liljegren et al. (2001) found RMS differences of 1-2 K for temperature. For absolute humidity the RMS differences averaged 0.25×10^{-3} kg m^{-3} in the lowest 2 km during the winter, 0.32×10^{-3} kg m^{-3} for spring, 0.14×10^{-3} kg m^{-3} for summer, and 0.23×10^{-3} kg m^{-3} for fall. The average biases were consistently positive, indicating that the MWRP measurements were slightly drier than the RAOBS for the lower 2 km. The sea ice concentrations of $9/10^{ths}$ and $10/10^{ths}$ have the lowest bias, which is to be expected with the least amount of open water present. Our results compare well to a study from Barrow, Alaska, where Liljegren et al. (2001) found the RMS differences for water vapour to be about 0.5×10^{-3} kg m^{-3} near the surface.

The vertical resolution as defined Smith et al. (1999) is the only method currently available, however the resolutions given are far too coarse compared to the resolution suggested by the statistical analysis of the individual seasons and as shown by the case study. The vertical resolutions calculated by the inter-level covariance method were in general as coarse as the height measured; at a height of 1 km the vertical resolution was approximately 1000 m.

Based on the statistical comparison of the MWRP with the RAOBS and the results of the direct comparison in the case study, the conclusion was drawn that MWRP does give reliable measurements for both temperature and absolute humidity.

The main objective of the thesis was to determine whether CloudSat and Calipso's data products can reliably be used to study cloud's in the high Arctic. The MWRP continuously measured the atmospheric temperature and absolute humidity directly above the Amundsen. Comparing CloudSat's ECMWF-aux data product to the MWRP, the temperature bias was positive except near the surface, which indicated that the ECMWF-aux data product gave warmer temperatures. Near the surface, the negative bias for temperature may be a factor of both the distance between the two measurements and the linear interpretation of the MWRP temperature and humidity data. The RMS difference for temperature showed a large difference between the two measurements, this led to the conclusion that the temperature should be viewed with skepticism. The absolute humidity RMS difference and bias showed good agreement over sea ice in the winter, which may be attributed to the Arctic's dry winter climate. During spring, summer and the fall the RMS differences for absolute humidity were substantially greater than during winter. This is likely due to greater variations in the ocean surface; sea ice concentrations ranged from $0/10^{ths}$ to $10/10^{ths}$ during the spring, summer and fall. The potential variability between the satellite's measurements and the ships location, which can be up to 50 km away, may have also led to the larger differences.

Cloud base heights are inherently difficult to compare when measurements are from two different locations. To compare the GeoProf-lidar data to the ship-borne data, measurements were used only when the satellite's ground track was within 50 km of the CCGS Amundsen. The large differences between the cloud base height measurements are likely due to the distance between the measurements.

There were 15 discrepancies when CloudSat and Calipso measured cloud while both the ceilometer and the MWRP saw clear skies for six hours. This is a large percentage considering there were only a total of 58 overlapping comparisons where both the MWRP and ceilometer were operational. This led to the hypothesis that the constraints used by the GeoProf-lidar algorithm for cloud detection may need to be refined to reduce the large number of false detections.

Future Directions

The MWRP was compared to RAOBS in the Beaufort Sea and Amundsen Gulf. The bias and RMS difference of the lower 4 km, for both temperature and absolute humidity was on the same order of magnitude as previous studies done in Alaska (Liljegren et al., 2001). Future field studies should use the MWRP to reliably measure the temperature and humidity profiles for the boundary layer in the Beaufort Sea and Amundsen Gulf. The data collected in future studies will be capable of capturing both seasonal trends and variations, as well as smaller scale trends over short time scales such as those used in case studies.

Both Smith et al. (1999) and Guldner and Spankuch (2001) suggest that the inter-level covariance method of calculating the vertical resolution is a lower limit. The statistical analyses of the MWRP data compared to the radiosondes and the case study led to the conclusion that the vertical resolution of the MWRP was much greater than that indicated by the inter-level covariance method. As such, future work should involve developing a new method to calculate the vertical resolution of a surface based microwave profiling radiometer.

Due to the nature of satellites and the constant degradation of their instruments, further validation is essential in the Arctic. Future studies should again compare cloud base heights and look to see if false detections continue to occur. Data comparisons of other satellite

products and surface based measurements should be conducted including comparing manual observations of cloud types to 2B-CLDCLASS-lidar, CloudSat and Calipso's combined cloud classification data product.

The Arctic climate has changed with air temperatures increasing 4 or 5 degrees in the Western Canadian Arctic and Alaska (Turner et al., 2007). The increased atmospheric temperature has lead to an increased surface temperature in the Arctic ocean. With these, an increase in evaporation is expected. Changes in the seasonal cloud cover is likely to occur in the Arctic. With a cloud's high albedo the potential is there to reduce the incoming solar radiation at the surface, which can decrease the rate of change of the surface temperatures, causing a negative feedback (Curry et al., 1996). However, the presence of clouds increases the reflected longwave radiation back to the surface and can limit the loss of radiative cooling, thus increasing the surface temperatures in a positive feedback (Curry et al., 1996). The changes in cloud cover as a result of changes in sea ice will effect the ice-albedo feedbacks and may contribute to the cloud-ice feedback during the early fall (Kay and Gettelman, 2009). Although the false detection rate of clouds was high for the GeoProf-lidar data product it was consistent for all seasons studied. Future studies can use CloudSat and Calipso's data products to study the seasonal trends and rate of change of clouds in the Arctic.

Satellite remote sensing represents the future of climate research. The data provided will allow for the Arctic to be studied consistently over long periods of time, and will further our understanding of Arctic climate change and it's impacts.

References

Barber, D. G., Asplin, M., Gratton, Y., Lukovich, J., Galley, R., Raddatz, R., and Leitch, D. (2010). The international polar year (ipy) circumpolar flaw lead (cfl) system study: introduction and physical system. *Atmos.- Ocean*.

Barry, R., Serreze, M., Maslanik, J., and Preller, R. (1993). The arctic sea ice-climate system: Observations and modeling. *Reviews of Geophys.*, 31(4):397.

Candlish, L. M., Raddatz, R., Asplin, M., and Barber, D. G. (2011). Veracity of atmospheric temperature and absolute humidity profiles over the beaufort sea and amundsen gulf from a microwave radiometer. *Journal of Atmospheric and Oceanic Technology - In Review*.

CIRA (2007). *CloudSat Project A NASA Earth System Science Pathfinder Mission: CloudSat Standard Data Products Handbook*. Cooperative Institute for Research in the Atmosphere, Colorado State University, Fort Collins, CO 80523.

Curry, J., Rossow, W., Randall, D., and Schramm, J. (1996). Overview of arctic cloud and radiation characteristics. *Journal of Climate*, 9(8):1731–1764.

Gaffard, C., Nash, J., Walker, E., Hewison, T. J., Jones, J., and EG, E. G. N. (2008). High time resolution boundary layer description using combined remote sensing instruments. *Ann. Geophys.*, 26:2597–2612.

Guldner, J. and Spankuch, D. (2001). Remote sensing of the thermodynamic state of the atmospheric boundary layer by ground-based microwave radiometry. *J. Atmos. and Oceanic Tech.*, 18:925–933.

Hahn, C., Warren, S., and London, J. (1995). The effect of moonlight on observation of cloud cover at night, and application to cloud climatology. *Journal of Climate*, 8(5):1429–1446.

Han, Y. and Westwater, E. (1995). Remote sensing of tropospheric water vapor and cloud liquid water by integrated ground-based sensors. *Journal of Atmospheric and Oceanic Technology*, 12(5):1050–1059.

Han, Y. and Westwater, E. (2002). Analysis and improvement of tipping calibration for ground-based microwave radiometers. *Geoscience and Remote Sensing, IEEE Transac-*

tions on, 38(3):1260–1276.

Isaac, G. and Stuart, R. (1996). Relationships between cloud type and amount, precipitation, and surface temperature in the mackenzie river valley-beaufort sea area. *Journal of Climate*, 9:1921–1941.

Jin, X., Hanesiak, J., and Barber, D. (2007). Time series of daily averaged cloud fractions over landfast first-year sea ice from multiple data sources. *Journal of Applied Meteorology and Climatology*, 46(11):1818–1827.

Jin, Z., Stamnes, K., Weeks, W., and Tsay, S. (1994). The effect of sea ice on the solar energy budget in the atmosphere-sea ice-ocean system: A model study. *J. Geophys. Res*, 99(C12):25–281.

Kay, J. and Gettelman, A. (2009). Cloud influence on and response to seasonal arctic sea ice loss. *Journal of Geophysical Research*, 114(D18):D18204.

Kay, J., L'Ecuyer, T., Gettelman, A., Stephens, G., and O'Dell, C. (2008). The contribution of cloud and radiation anomalies to the 2007 arctic sea ice extent minimum. *Geophysical Research Letters*, 35(8):L08503.

Liljegren, J., Lesht, B., Kato, S., and Clothiaux, E. (2001). Initial evaluation of profiles of temperature, water vapor and cloud liquid water from a new microwave profiling radiometer. In *Proceedings of the 5th Symposium on Integrated Observing Systems*.

Mace, G. (2007). Level 2 geoprof product process description and interface control document algorithm version 5.3. *NASA Jet Propulsion Laboratory*.

Mace, G., Vane, D., Stephens, G., and Reinke, D. (2007). Level 2 radar-lidar geoprof product version 0 - draft process description and interface control document level 2 radar-lidar geoprof product version 0 - draft process description and interface control document level 2 radar-lidar geoprof product version 0 - draft process description and interface control document level 2 radar-lidar geoprof product version 1 process description and interface control document. *NASA Jet Propulsion Laboratory*.

Maykut, G. (1978). Energy exchange over young sea ice in the central arctic. *Journal of Geophysical Research*, 83(C7):3646–3658.

Minnett, P. (1999). The influence of solar zenith angle and cloud type on cloud radiative forcing at the surface in the arctic. *Journal of Climate*, 12(1):147–158.

Overland, J. E. (2009). Meteorology of the beaufort sea. *J. Geophys. Res*, 114.

Overland, J. E. and Guest, P. S. (1991). The arctic snow and air temperature budget over sea ice during winter. *J. Geophys. Res*, 96:4651–4662.

Parkinson, C. (2003). Aqua: An earth-observing satellite mission to examine water and other climate variables. *Geoscience and Remote Sensing, IEEE Transactions on*, 41(2):173–183.

Partain, P. (2007). Cloudsat ecmwf-aux auxiliary data process description and interface control document. Technical report, California Institute of Technology, http://www.cloudsat.cira.colostate.edu/dataSpecs.php.

Schweiger, A. (2004). Changes in seasonal cloud cover over the arctic seas from satellite and surface observations. *Geophysical Research Letters*, 31(12):L12207.

Smith, W. L., Feltz, W. F., and and, R. O. K. (1999). The retrieval of planetary boundary layer structure using ground-based infrared spectral radiance measurements. *J. Atmos. and Oceanic Tech.*, 16:323–333.

Solheim, F., Godwin, J. R., Westwater, E. R., Han, Y., Keihm, S. J., March, K., and Ware, R. (1998). Radiometric profiling of temperature, water vapor, and cloud liquid water using various inversion methods. *Radio Science*, 33:393–404.

Stephens, G. and Kummerow, C. (2007). The remote sensing of clouds and precipitation from space: A review. *Journal of the Atmospheric Sciences*, 64(11):3742–3765.

Stephens, G., Vane, D., Boain, R., Mace, G., Sassen, K., Wang, Z., Illingworth, A., O'Connor, E., Rossow, W., Durden, S., et al. (2002). The cloudsat mission and the a-train. *Bulletin of the American Meteorological Society*, 83(12):1771–1790.

Tsay, S., Stamnes, K., and Jayaweera, K. (1989). Radiative energy budget in the cloudy and hazy arctic. *Journal of the Atmospheric Sciences*, 46(7):1002–1018.

Turner, J., Overland, J., and Walsh, J. (2007). An arctic and antarctic perspective on

recent climate change. *International Journal of Climatology*, 27(3):277–293.

Vaisala (2002). *Ceilometer CT25K User's Guide*. Vaisala, P.O. Box 26 FIN-00421 Helsinki, Finland, m210345en-a edition.

Vaisala (2003). *DigiCORA III MW21 Technical Documents*. Vaisala Oyj, P.O. Box 26 FIN-00421 Helsinki, Finland.

Vaughan, M., Young, S., Winker, D., Powell, K., Omar, A., Liu, Z., Hu, Y., and Hostetler, C. (2004). Fully automated analysis of space-based lidar data: An overview of the calipso retrieval algorithms and data products. *Proc. of SPIE Vol*, 5575:16–30.

Walsh, J. and Chapman, W. (1998). Arctic cloud-radiation-temperature associations in observational data and atmospheric reanalyses. *Journal of Climate*, 11(11):3030–3045.

Ware, R., Carpender, R., Guldner, J., Liljegren, J., Nehrkorn, T., Solhelm, F., and Vandenberghe, F. (2003). A multichannel profiler of temperature, humidity, and cloud liquid. *Radio Science*, 38:1–44.

A Appendix: Instruments

A.1 Microwave Profiler

The Radiometrics TP/WVP 3000 microwave radiometer (MWRP) provides high temporal resolution ($\approx$ 1 minute) atmospheric profiles for temperature (°K), and absolute humidity (10^{-3} kg m^{-3}) up to 10 km. The MWRP temperature and humidity values are volumetric measurements with a resolution of 50 meter intervals for 0 to 0.2 km, 100 meter intervals for 0.5 to 2 km, and 250 meters for 2 to 10 km. The MWRP uses 12 channels, with five channels in the 22–30 GHz range (oxygen band) and seven in the 51–59 GHz range (atmospheric water vapour absorption window). The radiometer has a viewing angle of 2–3 degrees in the oxygen band and 5–6 degrees in the water vapour band, giving an inverted cone observation (Ware et al., 2003). The 12 frequencies shown in Table A 1, were determined using eigenvalue analysis to optimize the profile (Solheim et al., 1998). The profiles are processed in real-time giving continuous monitoring of the lower troposphere interrupted only during moderate to heavy precipitation and emissions from moisture on the radome.

Table A 1: The frequency of each channel for the TP/WVP 3000 microwave profiler. Adapted from Guldner and Spankuch (2001).

Frequency (GHz)	Beamwidth (°)	Absorption Window
22.235		
23.035		water vapour &
23.835	5.5	cloud liquid water
26.235		
30.000	4.5	
51.250		
52.280	2.7	
53.850		
54.940		oxygen band &
56.660		temperature
57.290		
58.800	2.3	

The MWRP uses passive microwave radiometry with seven channels in the oxygen band (51–59 GHz) to determine the temperatures. The mixing ratio of oxygen is constant with height, thus the received emission is dependent on the temperature (Han and Westwater, 2002). The seven different frequency channels are used to receive the emissions from a range of altitudes, which give the vertical distribution of temperature. The atmospheric water vapour is determined using five channels in the 22–30 GHz range, the water vapour absorption band. The five different frequencies have different responses to the water vapour and liquid water and thus give differentiating brightness temperatures. From the brightness temperatures the water vapour profiles, perceptible water vapour and integrated cloud liquid water are derived. These values were derived from microwave brightness temperatures using the manufacturer's neural network retrieval and radiative transfer model. The neural network is trained by historical radiosonde data ($\approx$ 10,000) from the upper-air station in Inuvik, Canada (68.30 °N; 133.47 °W). The neural network is a forward model, which uses a standard back propagation algorithm for training with the RAOBS. The basis of the neural network uses Planck's Law and Stefan-Boltzman's Law to determine the atmospheric temperature and humidity from the brightness temperature.

The water vapour profiling channels are calibrated hourly with tipping curves (Guldner and Spankuch, 2001). The tipping curve method calibrates the radiometer system by coupling the radiative transfer equations with the radiometer equations. For a tipping calibration, two or more measurements are taken from different elevation angles in a clear, horizontally-stratified atmosphere. The calibration uses an iteration where the adjustments of a single parameter is performed until the output of the system is acceptable. An external liquid nitrogen blackbody target is used to intermittently calibrate the temperature channels. All twelve channels perform a relative calibration every 5 minutes by viewing an internal black body target.

The MWRP also contains a sensor for surface pressure, and a zenith-pointing infrared ra-

diometer (9.6–11.5 μm) (Ware et al., 2003). The cloud base height is estimated from the infrared observations of the cloud base temperature and from the retrieved temperature profile (Ware et al., 2003). The cloud base height and temperature is also needed to constrain the water vapour and liquid water retrievals (Han and Westwater, 1995).

A.2 Ceilometer

The Vaisala CT25K Ceilometer is a ground based instrument that uses LIDAR technology to detect the cloud base height for up to 10 km (25,000 feet) and 3 layers of clouds. Besides cloud layers it can detect if there is precipitation or an obstruction to the viewing field. The ceilometer operates by measuring the time needed for the laser pulse to travel from the transmitter to a backscattering cloud base and back to the receiver in the ceilometer.

Particles at all heights will cause a backscatter from the laser pulse. The magnitude of the return signal provides information about fog and precipitation. Since the fog and precipitation will attenuate the pulse, the cloud base will appear lower in magnitude in the return echo. The ceilometer digitally samples the return echo every 100 ns from 0 to 50 μs, giving a spatial resolution of 50 ft ($\approx$ 15 m) from the ground to 25,000 ft ($\approx$ 7.6 km) (Vaisala, 2002).

The ceilometer uses a low laser power such that the noise of the ambient light exceeds the return signals. To compensate for this, many laser pulses are used and the backscattered signals are summed. The large number of pulses multiplies the desired signal, whereas the random noise is partially cancelled out. The resulting signal-to-noise ratio improvement is equal to the square root of the number of pulses. The number of samples is limited however due to the changes or movement of the clouds and environment (Vaisala, 2002).

The lidar equation for the ceilometer is given in the general form (Vaisala, 2002):

$$Pr(z) = E_0 . \frac{c}{2} . \frac{A}{z^2} . \beta(z) . e^{-2 \int \sigma(z') dz'}$$

Where:

$Pr(z)$ Is the instantaneous power received from distance z (in Watts)

E_0 Is the effective pulse energy (in Joules)

c Is the speed of light (in m/s)

A Is the receiver aperture (in m^2)

z Is the distance in question (in m)

$\beta(z)$ Is the volume backscatter coefficient at distance z (in $m^{-1}strad^{-1}$)

$e^{-2\int\sigma(z')dz'}$ Is the two way atmospheric transmittance and accounts for the attenuation of transmitted and backscattered power by extinction at various distances (z') between transceiver and distance in question (z).

The expression equals 1 in a clear atmosphere.

The equation states that the reflection of light backscatter caused by haze, fog, mist, virga, precipitation, and clouds is measured as the laser pulses traverse the sky. The resulting backscatter profile (i.e., signal strength versus height) is stored. Based on the time delay between the launch of the laser pulse and the backscatter signal and knowing the speed of light, the cloud base height is calculated. The data is archived hourly as an ASCII file.

A.3 Radiosondes

The Vaisala RS92 radiosonde and Digicora III software was used to collect vertical profiles of temperature, pressure, relative humidity, wind speed and wind direction. The wind speed and direction are given based on the GPS data. The radiosonde ground station was located in the met shack behind the bridge. All balloons were launched off the helicopter flight deck with 350g Totex balloons with a target ascent rate of 5 m/s to ensure a good vertical resolution through the boundary layer.

The RS92 has an uncoded 12-channel GPS receiver in each sonde. The wind data is given by using the carrier phase measurements and the Doppler frequency. The Doppler shift is caused by the relative motion between the radiosonde and the satellite and is on the order of $\pm$ 5 KHz. The temperature sensor is a THERMOCAP capacitive wire, which has a +60 °C to -90 °C range, a response time of <0.4 s at 1000 hPa and ascending at 6 m/s. It has a resolution of 0.1 °C and a total uncertainty accuracy of 0.5 °C in the sounding. The humidity is measured using a thin-film capcitor with a heated twin sensor. The measurement range is from 0 to 100% RH, with a resolution of 1 %. The response time is <20 s at -40 °C with an ascent rate of 6 m/s and at 1000 hPa. The RS92-SGPD uses a silicon pressure sensor. The measurement range is from 1080 hPa to 3 hPa with a resolution of 0.1 hPa. The total uncertainty in the sounding from 1080 – 100 hPa is 1 hPa (Vaisala, 2003).

The RS92-SGPD uses 9V alkaline batteries, and a synthesized transmitter. The RS92 uses the frequency band of 403 MHz, with a tuning range of 400–406 MHz to transmit the data to the ground unit. The base station uses the Vaisala ground check set GC25. The system reads the calibration coefficients automatically. The ground check unit is used to recondition the humidity sensor and remove any chemical contaminants (Vaisala, 2003).

A.4 CloudSat and Calipso

The A-Train is a series of polar orbiting satellites currently led by Aqua, which was launched in 2004 (Parkinson, 2003). The A-Train presently has satellites Aqua, CloudSat, Calipso and Aura. In December 2009, Parasol exited the constellation. NASA's Glory was launched in March 2011 but failed to reach orbit. All the satellites in the A-Train have unique abilities to measure atmospheric variables, with many of the capabilities complimenting one another. The A-Train is the first satellite constellation capable of measuring aerosols, clouds, atmospheric temperature and humidity and radiative fluxes nearly simultaneously. NASA, jointly with Colorado State University, use data from Aqua and Calipso to combine with CloudSat's Cloud Profiling Radar (CPR) for more accurate and in depth vertical structure of clouds and the atmosphere.

Table A 2 describes each of the current satellites, their place in the constellation, along with the instruments onboard each of the satellites and the cloud and aerosol data products.

Table A 2: Sensor complement and related products of the A-Train. Adapted from Stephens et al. (2002).

Spacecraft	**Payload**	**Characteristics**	**Cloud and Aerosol Products**
Aqua Lead constellation spacecraft	MODIS	36-channel visible radiometer, 2300-km-wide swath, variable resolution from 0.25 to 1 km.	Land, ocean, and atmospheric products. The latter include cloud and aerosol optical depths and particle size information, as well as cloud emissivity and cloud-top height.
	AIRS/ AMSU-A /HSB	Combination of IR and microwave sounders. swath of $\pm$ 50°, resolution of IR sounder $\approx$10 km.	Temperature and moisture profiles in clear atmosphere. Some cloud properties.
	AMSR-E	6-channel microwave radiometer. 1445 km swath, asymmetric FOV with variable resolution from $\approx 6^\circ$ – 4 km (89 GHz) to $\approx 43^\circ$ –75 km (6 GHz)	LWP, column water vapour, liquid precipitation, principally confined to ocean regions.
	CERES	Broadband and spectral radiances converted to fluxes, resolutions at nadir – 20 km.	TOA radiation budget. Primary product is time mean fluxes but instantaneaous fluxes are also produced.

Continued on Next Page...

Table A 2 – Continued

Spacecraft	Payload	Characteristics	Cloud and Aerosol Products
CloudSat Lags Aqua by a variable amount less than 120 s	94 GHz radar (CPR)	500 m vertical range gates from surface to 30 km. High sensitivity, FOV ≈1.4 km.	Cloud profile information, liquid and ice water content profiles, precipitation. The data products use a combination of the radar measurements, MODIS and AMSR-E, as well as Calipso's lidar.
Calipso Lags CloudSat by 15 ± 2 s.	Lidar (CALIOP)	532 and 1064 nm channels with depolarization. FOV of ≈300 and 70 m resolution.	Cloud profile information, primarily of upper tropospheric clouds. Optical depth of thin cirrus. Aerosol profiles with attached optical depth estimates.
	IIR	3 channel IR radiometer with a FOV of 1 km swath of 64 km.	Cirrus cloud optical properties
Aura Lags Aqua by ≈ 15 min.	HIRDLS	IR limb sounder.	Trace gases and stratospheric aerosol.
	MLS	Microwave limb sounder.	Trace gases, ice content of thin upper-tropospheric cloud.
	TES	IR imaging spectrometer, 0.5 x 5 km resolution, narrow	Trace gases, could also provide high spectral resolution data on clouds.

Continued on Next Page...

Table A 2 – Continued

Spacecraft	Payload	Characteristics	Cloud and Aerosol Products
		swath and variable pointing.	
	OMI	UV grating spectrometer, 13 x 24 km resolution.	Ozone and aerosol index.

A.4.1 CloudSat

CloudSat is a NASA funded Earth Sciences Systems Pathfinder (ESSP) mission with the principal investigator Dr. Graeme Stephens of Colorado State University. CloudSat's mission is to measure the vertical structure of clouds and simultaneously observe clouds and precipitation (CIRA, 2007). CloudSat has the first spaceborne millimeter wavelength radar. The millimeter radar has the unique function to measure both the cloud condensate and precipitation within its nadir field of view (Stephens et al., 2002). Global atmospheric circulation models need cloud properties for accuracy; CloudSat's mission is the first to evaluate the representation of clouds and cloud processes in these models. CloudSat also looks at the vertical profiles of cloud liquid water and ice content and their correlation with cloud radiative properties.

CloudSat and the A-Train provide new information on aerosols and their role in the changing

cloud properties and radiative budget of clouds. The combination of data from the various A-Train systems provides vital information about aerosol-chemistry-cloud interactions (Stephens et al., 2002).

CloudSat produces 11 data products, with the standard products shown below in Table A 3. The data products are produced through the combination of CloudSat's cloud profiling radar with data from several other sources, including ECMWF, MODIS, CALIPSO, and AMSR.

Table A 3: CloudSat's standard data products Adapted from CIRA (2007).

Product	Description
1B-CPR and 1B-CPR-FL	Radar Backscatter Profiles
2B-GEOPROF	Cloud Geometrical Profile
2B-CLDCLASS	Cloud Classification
2B-CWC-RO	Combined Water Content- Radar Only
2B-TAU-OFF-N	Cloud Optical Depth Off Nadir
2B-CWC-RVOD	Combined Water Content Radar + Vis Optical Depth
2B-FLXHR	Fluxes and Heating Rates
2B-GEOPROF-LIDAR	Cloud Geometrical Profile from CPR and CALIPSO Lidar
2B-CLDCLASS-LIDAR	Cloud Classification from CPR and CALIPSO Lidar

CloudSat has the first spaceborne Cloud Profiling Radar (CPR). The CPR is a 94-GHz nadir-viewing radar that is designed after NASA's Airborne Cloud Radar, which has been operating on the NASA DC-8 aircraft since 1998. The CPR has a sampling rate of 625 kHz with an instantaneous footprint of 1.4 km at mean sea level. Figure A 1 shows a CloudSat data granule.

A CloudSat granule is one orbit of data beginning at the equator on the descending path. Each granule is made up of approximately 36, 383 profiles and each profile is made up of 125 vertical bins. A vertical bin is 240 m thick with 1.1 km along-track interval and a 1.4 km by 2.5 km footprint.

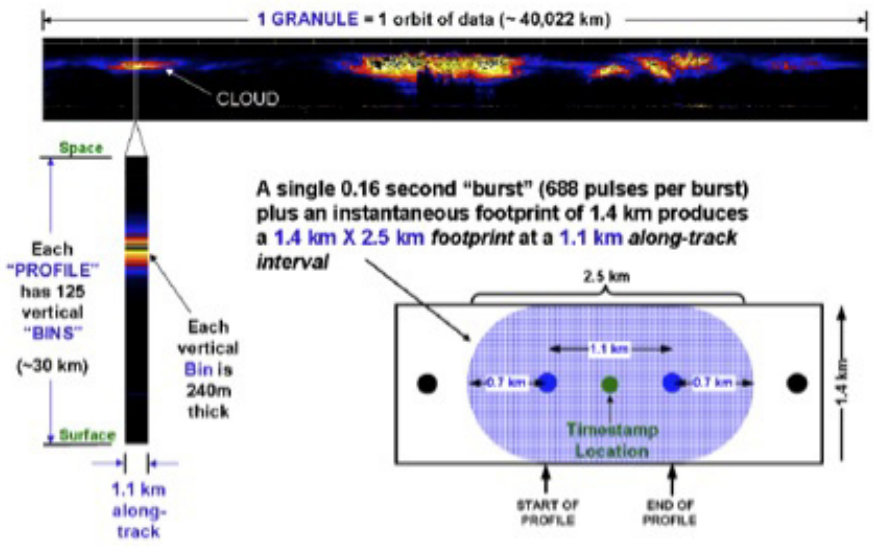

Figure A 1: CloudSat data footprint and granule size (CIRA, 2007).

CloudSat has two types of data products, Standard Data Products, Table A 3 and Auxiliary Data Products. Each data product is generated for every profile location. Auxiliary products are mapped to the horizontal center of each CloudSat profile and where needed the vertical center of each bin. The auxiliary data product 1A-AUX contains engineering data, time, geolocation and elevation for each CPR level.

A.4.2 Calipso

Calipso's main instrument is the Cloud-Aerosal LIdar with Orthogonal Polarization (CALIOP). CALIOP detects vertical profiles of electrical backscatter at both 1064nm and 532nm from a near nadir-viewing geometry (Vaughan et al., 2004). Calipso can determine aerosol and cloud heights profiles from the total backscatter measurements. CALIOP also provides profiles of linear depolarization at 532 nm. This allows for the distinction between ice clouds

and water clouds and the identification of non-spherical aerosol particles. Along with the two-wavelength polarization-sensitive lidar, Calipso has two passive imagers operating in the visible and infrared spectral regions. These instruments are capable of measuring the vertical distributions of clouds and aerosols in the atmosphere, along with the optical and physical properties of the aerosols and clouds (Vaughan et al., 2004). Calipso has three main objectives: 1) to improve observationally-based estimates of direct and indirect aerosol radiative forcing, 2) to improve characterization of surface longwave radiative fluxes and atmospheric heating rates, and 3) to improve model parameterizations of cloud-climate feedbacks (Vaughan et al., 2004).

The resolution of Calipso's lidar (as determined by the receiver electrical bandwith and the laser pulse repetition) is 333m horizontal and 30m vertical.

Table A 4: Spatial resolutions for the Calipso on-board averaging scheme. Adapted from Vaughan et al. (2004).

Base (km)	Top (km)	Vertical Resolution (m)	Horizontal Resolution (m)	Profiles per 5km	Samples per Profile
40.0	30.1	300	5000	1	33
20.2	30.1	180	1667	3	55
8.2	20.2	60	1000	5	200
-0.5	8.2	30	333	15	290
-2.0	-0.5	300	333	15	5

Table A 4 details how the averaging varies with altitude. An on-board altitude dependent averaging scheme gives full resolution in the lower troposphere and lower resolution in the higher atmosphere. This averaging scheme is used because the variability of clouds and aerosols is highest in the lower troposphere and the atmosphere becomes more uniform with increasing height.

Calipso data products are divided into three groups: a vertical feature mask, cloud and aerosol layer products and profile products. The vertical feature mask provides the spatial distribution features. The cloud and aerosol layer products provide numerical descriptions of

all the features detected. The profile products map the vertical distributions of backscatter and extinction coefficients (Vaughan, et al., 2004).

The layer products provide a listing of all features detected in a horizontal column and contain layer-integrated optical properties for each layer. The layer product is made up of column descriptors and layer descriptors (Vaughan et al., 2004). The column descriptors give the time and geophysical location of the atmospheric column and include data about the surface. Each feature in a column is given a layer descriptor. The layer descriptor provides spatial and optical properties, and includes base and top altitudes, integrated backscatter, lidar ratio and optical depth. Calipso layer products have a minimum horizontal averaging resolution of 5km and for cloud layer products they also have resolutions of 1/3 km and 1 km (Vaughan, et al., 2004). The higher resolution cloud layer products only report data from clouds that were strong enough to be detected at the corresponding resolution. Table A 5 and Table A 6 provide a detailed list of the column descriptors and layer descriptors.

Table A 5: Calipso column descriptors. Adapted from Vaughan et al. (2004).

Column Parameter	Description
1B-CPR and 1B-CPR-FL	Radar Backscatter Profiles
Profile ID	Unique integer identifier associated with each laser pulse
Latitude & longitude	Latitude and longitude of the laser footprint
Profile time	Laser firing time and date
Day/night flag	Lighting conditions at the surface
Solar zenith and azimuth angle	
Sensor nadir angle	
532 column reflectance	Reflectance's derived from 532 nm parallel and perpendicular channel background monitors and associated uncertainty
Tropopause height and temperature	Obtained from NASAs Global Modeling and Assimilation Office
IGBP surface type	Surface type derived from the International Geosphere-Biosphere Programme (IGBP) database
DEM surface elevation	Height of surface at the footprint location derived from a digital elevation map
Lidar surface elevation	Height of surface determined from lidar return (if found)
Number of layers found	From 0 to a maximum of 15

Table A 6: Calipso layer descriptors. Adapted from Vaughan et al. (2004).

Layer Parameter	Description
Base & top altitudes	Layer base and top heights, in kilometers.
Opacity flag	If feature transmissive or opaque.
Horizontal averaging	SIBYL horizontal averaging level at which the layer was detected.

Continued on Next Page...

Table A 6 – Continued

Layer Parameter	Description
Total attenuated backscatter statistics at 532 nm	Integrated attenuated backscatter and associated uncertainty; also, the minimum, maximum, mean, standard deviation, centroid, and skewness of the 532 nm attenuated total backscatter computed between feature base and feature top.
Total attenuated backscatter statistics at 1064 nm	Integrated attenuated backscatter and associated uncertainty; also, the minimum, maximum, mean, standard deviation, centroid, and skewness of the 1064 nm attenuated total backscatter computed between feature base and feature top.
Volume depolarization ratio statistics	Layer-integrated volume depolarization ratio and associated uncertainty; also, the minimum, maximum, mean, standard deviation, centroid, and skewness of the volume depolarization ratios computed between feature base and feature top.
Attenuated total color ratio statistics	Layer-integrated attenuated total color ratio and associated uncertainty; also, the minimum, maximum,

Continued on Next Page...

Table A 6 – Continued

Layer Parameter	Description
	mean, standard deviation, centroid, and skewness of the attenuated total color ratios between feature base and feature top.
Feature classification flags	Includes cloud/aerosol classification and ice/water phase discrimination.
Measured two-way transmittance at 532 nm (T^2, $\triangle T^2$)	For transmissive features, the mean attenuated scattering ratio beneath the feature and its associated uncertainty.
Two-way transmittance measurement region	For transmissive features, the base and top altitudes of the region beneath the feature where the two-way transmittance was measured.
Feature optical depth at 532 nm	Calculated 532 nm optical depth and associated uncertainty.
532 nm lidar ratio	Final 532 nm lidar ratio as reported by HERA.
Feature optical depth at 1064 nm	Calculated 1064 nm optical depth and associated uncertainty.
1064 nm lidar ratio	Final 1064 nm lidar ratio as reported by HERA.

A.4.3 ECMWF-aux Data Product

The ECMWF-aux product is generated from data produced by the European Center for Medium Range Weather Forecasting (ECMWF) global data set. The ECMWF data is interpolated into the CloudSat vertical bins and is required for input into the 2B-GEOPROF, 2B-CLDCLASS, 2B-TAU, and 2B-FLXHR algorithms (CIRA, 2007).

The geolocation data from the 1B-aux product is used with an interolate-to-reference algorithm to find the four bounding ECMWF grid points around the CloudSat bin which is then linearly interpreted. The ECMWF data is forecasted multiple times per day, thus the two forecasts that bound the CloudSat profile are used in a temporal interpretation, which results in the ECMWF-aux data product (Partain, 2007). The temperature is increased at a constant lapse rate of 6.5 K/km, while pressure is increased using a hyposemtric equation (Partain, 2007).

The ECMWF-aux output data is in HDF-EOS 4 files. Missing values occur only in bins that are below the surface of the Earth. Table A 7 gives the data fields available in the ECMWF-aux data product.

Table A 7: ECMWF-aux data fields. Adapted from Vaughan et al. (2004).

Field	Description
Profile Time	Seconds since the start of the granule. The first profile is 0.
UTC Start	The UTC seconds since 00:00 Z of the first profile in the data file.
TAI start	The TAI (International Atomic Time) timestamp for the first profile.
Latitude	Spacecraft Geodetic Latitude
Longitude	Spacecraft Geodetic Longitude
EC Height	Idealized height of the ECMWF data bin, where bin 105 is at MSL.
DEM elevation	Elevation in meters above MSL.
Extrapolation flag	A bit field that indicates areas where ECMWF data are extrapolated to fill in CPR bins that occur below the lowest ECMWF layers.
Pressure	Atmospheric Pressure in Pa.
Temperature	Atmopsheric temperature in K.
Specific humidity	Specific Humidity in kg/kg.
Ozone	Ozone in kg/kg.
Surface pressure	Atmospheric Pressure at the surface in Pa.
Skin temperature	Skin temperature in K.
Temperature 2m	Two-meter temperature in K.

A.4.4 GeoProf-lidar Data Product

2B-GeoProf-lidar is a combined data product from CloudSat's CPR and Calipso's CALIOP (lidar). The CPR has the ability to detect optically thick large-particle layers and with the lidar's ability to sense optically thin layers and weak cloud tops a combined data product has the potential to profile the complete atmosphere. The GeoProf-lidar data product aims to provide the best description of the occurrence of hydrometeor layers as well as the fractional volume of clouds (Mace et al., 2007).

CloudSat and Calipso have different vertical and horizontal resolutions, with CloudSat's CPR having a footprint of 1.4 km by 2.5 km and a vertical resolution of approximately

0.25 km and Calipso's lidar having a footprint of 0.3 km by 0.3 km to 1 km and a variable vertical resolution of 0.03 km to 8.2 km. The GeoProf-lidar algorithm uses the spatial grid determined by the CPR (Mace et al., 2007). The overlap of the radar and lidar is shown in Figure A 2. Due to finer spatial resolution the lidar will be deferred to for the cloud base height and cloud top height. If the cloud top is identified by lidar but signal attenuates, the radar will define the cloud base height (Mace et al., 2007). The lidar may falsely label aerosol layers as clouds. Boundary layer aerosols are consistently classified as clouds in certain conditions, the newest product release tried to resolve this issue (Mace et al., 2007).

The GeoProf-lidar output data is in HDF-EOS-4 files. Table A 8 describes each of the fields.

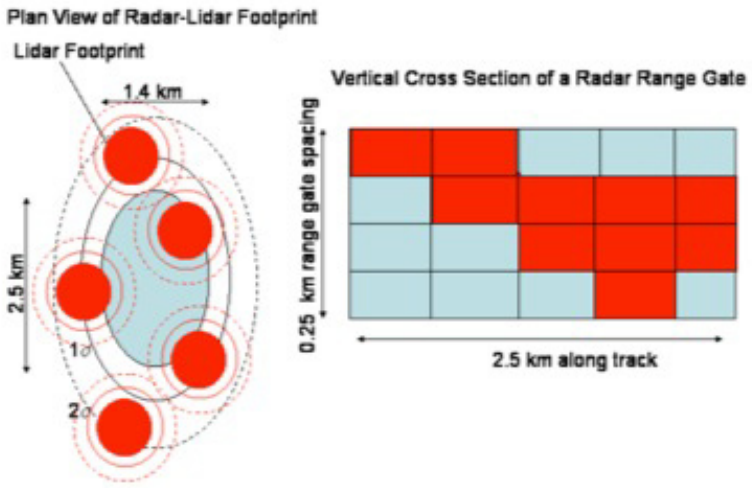

Figure A 2: A conceptual image of the radar-lidar overlap. The left image shows the radar footprint in blue with the lidar footprint in red. The black/red lines represent the standard deviation with the dashed lines representing the 2nd standard deviation. The right image is the vertical cross section of the radar range volume. The red squares represent the lidar resolution volumes. Adapted from Mace et al. (2007).

Table A 8: 2B-GeoProf-lidar data fields. Adapted from Mace (2007).

Field	Description
Profile Time	Seconds since the start of the granule. The first profile is 0.
UTC Start	The UTC seconds since 00:00 Z of the first profile in the data file.
TAI start	The TAI (International Atomic Time) timestamp for the first profile.
Latitude	Spacecraft Geodetic Latitude
Longitude	Spacecraft Geodetic Longitude
Height	Height of the radar range bins in meters above mean sea level.
Range to intercept	Range from the spacecraft to the CPR boresight intercept with the geoid, units in km.
DEM elevation	Elevation in meters above MSL.
Vertical Binsize	Effective vertical height of the radar range bin in m.
Pitch offset	Nominal satellite pitch offset from nadir. (Degrees)
Roll offset	Nominal satellite roll angle offset from nadir. (Degrees)
Data quality	Flags indicating data quality. If 0, then data is good quality.
Data status	Data status flags.
Data targetID	The target id indicates the orientation of the spacecraft bus.
CloudFraction	The CloudFraction reports the fraction of lidar volumes in a radar resolution volume that contains hydrometeors (between 0 and 100%)
UncertaintyCF	Quality of radar and lidar data.
CloudLayers	Number of hydrometeor layers in the vertical column.
LayerBase	Height of layer base in m.
LayerTop	Height of layer top in m.
FlagBase	Flag of layer base indicating if either the CPR or lidar find a base.
FlagTop	Flag of layer top indicating if either the CPR or lidar find a top.

B Appendix: Ceilometer Data 2009 and 2010

The ceilometer data was thought to be suspect previous to a routine calibration performed by Vaisala in March 2010. The cloud base height data for approximately 15 days from October 2009 and October 2010 were compared to see if there was a substantial difference. Figures B 1 and B 2 show the absolute humidity, with the hourly median cloud heights measured by the ceilometer and MWRP during the 15 day time period for 2009 and 2010. The two figures don't show a substantial difference between the two years. The MWRP generally measures more high clouds, while the ceilometer measures clouds closer to the ground.

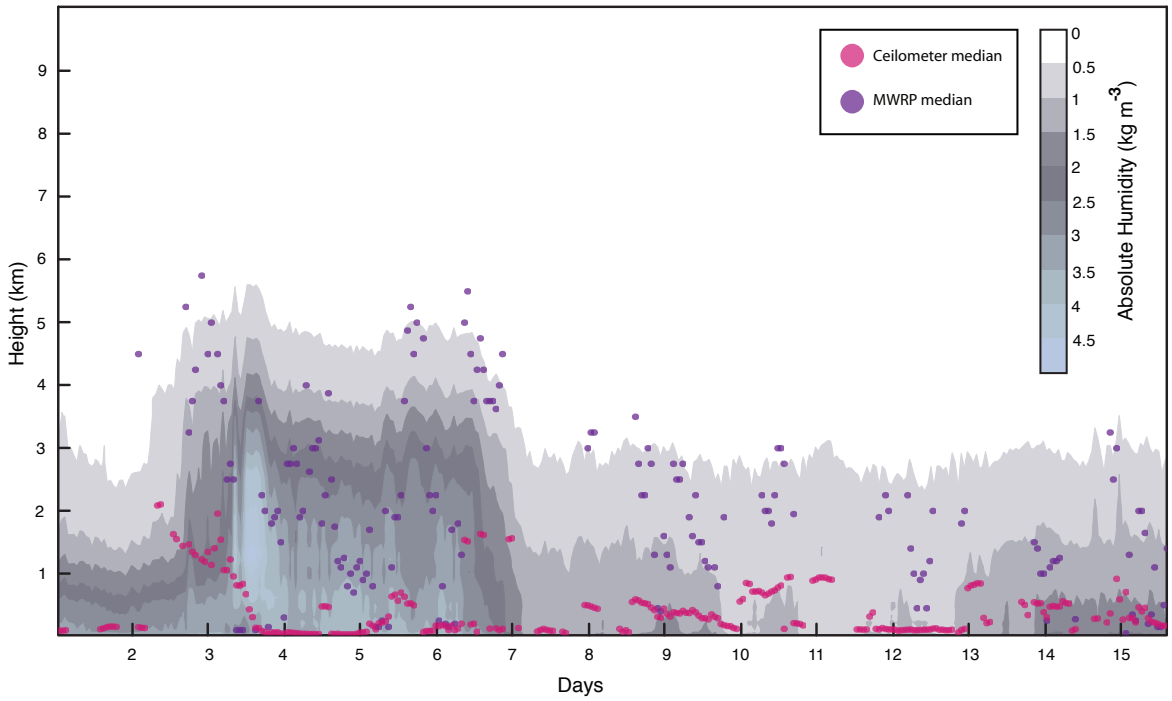

Figure B 1: The absolute humidity with cloud heights for fifteen days in October 2009.

There were a total of 350 comparable measurements. Table B 1 lists the total operational hours, total cloud free hours and the total hours for low, middle and high clouds during each of the 15 days in October 2009 and 2010. The ceilometer doesn't show a substantial difference from before the calibration and after. The major difference is the amount of cloud

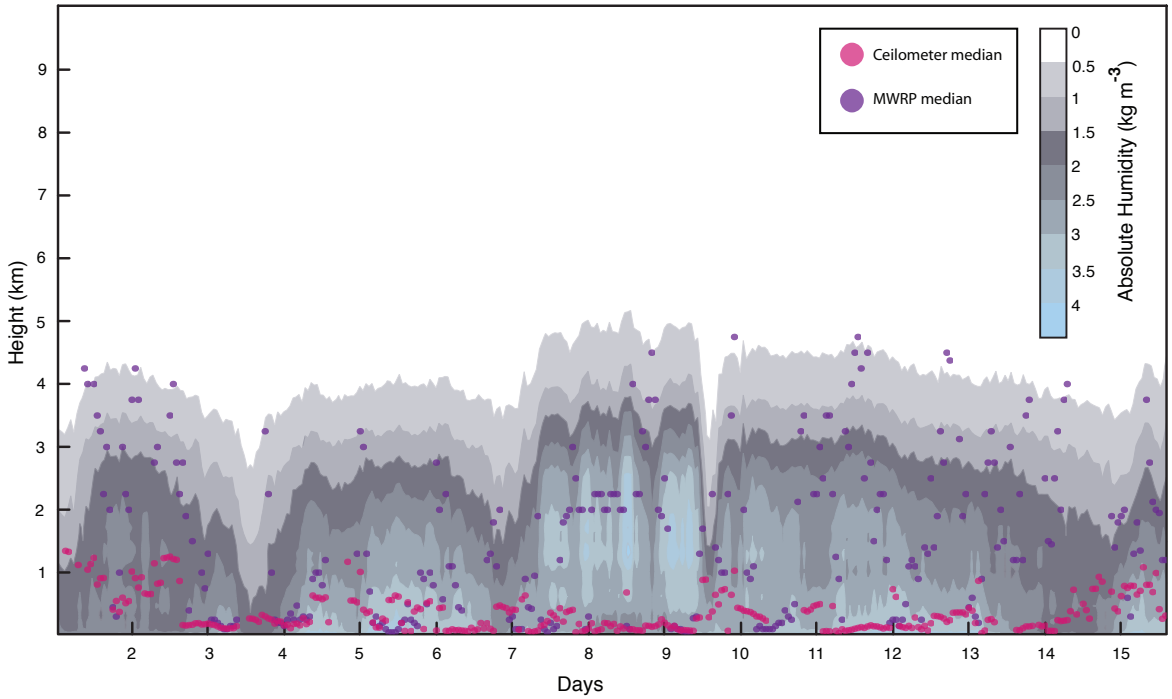

Figure B 2: The absolute humidity with cloud heights for fifteen days in October 2010.

free hours it measured, which can easily be due to the temporal and spatial variability of clouds. Figure B 3 shows the frequency distribution of the bias, MWRP minus ceilometer, for each year. The distribution data were divided into class intervals with a width of 500 meters, centered on 0. The purple bar shows the occurrences when the MWRP had clear skies and the ceilometer measured clouds. Similarly the pink bar is the number of occurences when the MWRP detected clouds and the ceilometer showed clear skies. There is a difference between 2009 and 2010 in the number of times the the MWRP showed clear skies and the ceilometer did not; this is likely due to year-to-year variability. The zero interval includes all measurements when both the MWRP and ceilometer measured clear skies. Both years have a nearly normal distribution with a positive skewness. This indicates that the ceilometer generally measured lower cloud than the MWRP.

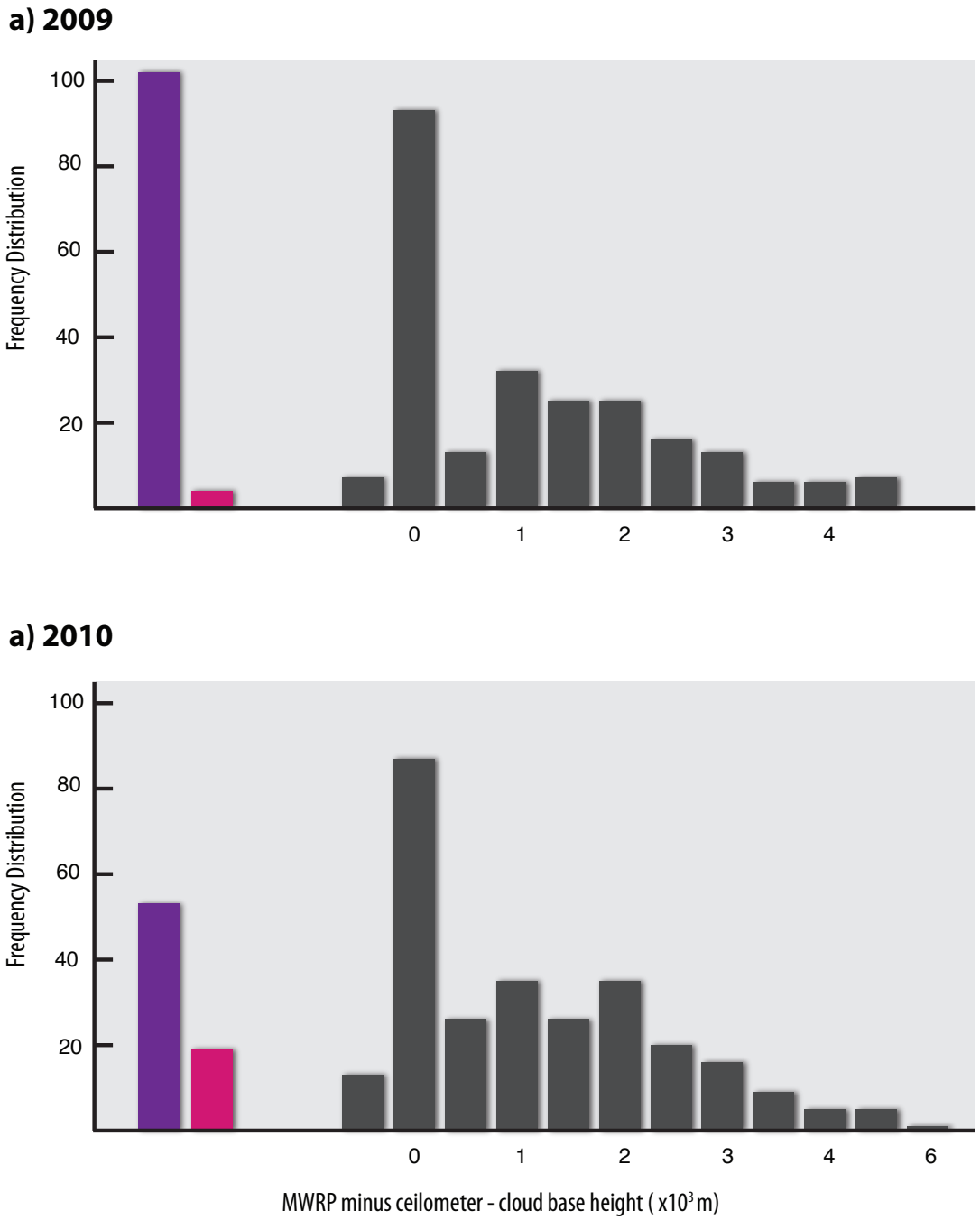

Figure B 3: The frequency distribution of the ceilometer bias, MWRP minus ceilometer. The ceilometer and microwave profiler use the median cloud base height over an hour. The purple indicates occurrences when the ceilometer measured clouds and the MWRP had clear skies. Likewise, the pink indicates occurrences when the ceilometer had clear skies and the MWRP measured clouds.

Table B 1: The hourly median cloud base height as measured by the MWRP and ceilometer. Each value is in hours.

	2009	2010
Operational Hours	350	350
MWRP Data		
Cloud Free	175 (50.0%)	71 (20.3%)
Low Clouds	101 (28.9%)	189 (54.0%)
Mid Clouds	55 (15.7%)	80 (22.9%)
High Clouds	19 (5.4%)	10 (2.9%)
Ceilometer Data		
Cloud Free	77 (22.0%)	38 (10.9%)
Low Clouds	271 (77.4%)	312 (89.1%)
Mid Clouds	2 (0.6%)	0 (0.0%)
High Clouds	0 (0.0%)	0 (0.0%)

Although there are some differences in the analysis of the 2009 date versus the 2010 data it is not a substantial difference and may be due to the year-to-year variability of clouds. Based on the analysis, the ceilometer data, prior to the calibration, was acceptable.

C Appendix: Additional Contributions

In addition to the two manuscripts that comprise this thesis, I also co-authored two additional journal articles.

Raddatz R.L., M.G. Asplin, L. Candlish and D.G. Barber, 2010. General Characteristics of the Atmospheric Boundary Layer Over a Flaw Lead Polynya Region in Winter and Spring, Boundary-Layer Meteorology, 138(2): 321-335

For Raddatz et. al., (2010) I helped with the collection of the field data, and the comparison of the MWRP data with the radiosondes.

Asplin M.G., L.M. Candlish, R.J. Galley, R.L. Raddatz and D.G. Barber, 2011. A Surface-to-Environment Synoptic Typing Approach To Classify Cyclone Forcing of Ocean-Sea Ice-Atmosphere Coupling within the Cape Bathurst Flaw Lead. Prepared for submission to Journal of Geophysical Research - Oceans.

For Asplin et. al., I was involved with the collection of the field data and quality assurance.